DMD Fast Forward. Published on March 3, 2015 as DOI: 10.1124/dmd.114.062539
This article has not been copyedited and formatted. The final version may differ from this version.

Towards Predicting Drug-Induced Liver Injury (DILI): Parallel Computational Approaches to Identify MRP4 and BSEP Inhibitors

Matthew A. Welch, Kathleen Köck, Thomas J. Urban, Kim L. R. Brouwer, and Peter W. Swaan

Department of Pharmaceutical Sciences, University of Maryland, Baltimore, Maryland (M.A.W., P.W.S.); Division of Pharmacotherapy and Experimental Therapeutics, UNC Eshelman School of Pharmacy, The University of North Carolina at Chapel Hill, Chapel Hill, North Carolina (K.K., T.J.U., K.L.R.B.); Center for Human Genome Variation, Duke University Medical Center, Durham, North Carolina (T.J.U.)

DMD Fast Forward. Published on March 3, 2015 as DOI: 10.1124/dmd.114.062539
This article has not been copyedited and formatted. The final version may differ from this version.

Running Title: Computational Modeling of MRP4 and BSEP to Predict DILI

Corresponding author: Peter W. Swaan, Ph.D., Department of Pharmaceutical Sciences, University of Maryland, Baltimore MD 21201. Tel. 410-706-0103. Email pswaan@rx.umaryland.edu

Number of text pages: 34

Figures: 9

Tables: 2

Number of References: 26

Number of Words in

Abstract: 249

Introduction: 693

Discussion: 1,356

Abbreviations: BSEP, bile salt export pump; DILI, drug-induced liver injury; PFIC, progressive familial intrahepatic cholestasis; MRP, multidrug resistance protein

DMD Fast Forward. Published on March 3, 2015 as DOI: 10.1124/dmd.114.062539
This article has not been copyedited and formatted. The final version may differ from this version.

Abstract

Drug-induced liver injury (DILI) is an important cause of drug toxicity. Inhibition of MRP4, in addition to BSEP, might be a risk factor for the development of cholestatic DILI. Recently, we demonstrated that inhibition of MRP4, in addition to BSEP, may be a risk factor for the development of cholestatic DILI. Here, we aimed to develop computational models to delineate molecular features underlying MRP4 and BSEP inhibition. Models were developed using 257 BSEP and 86 MRP4 inhibitors and non-inhibitors in the training set. Models were externally validated and used to predict the affinity of compounds towards BSEP and MRP4 in the DrugBank database. Compounds with a score above the median fingerprint threshold were considered to have significant inhibitory effects on MRP4 and BSEP. Common feature pharmacophore models were developed for MRP4 and BSEP with LigandScout software using a training set of 9 well-characterized MRP4 inhibitors and 9 potent BSEP inhibitors. Bayesian models for BSEP and MRP4 inhibition/non-inhibition were developed with cross-validated Receiver Operator Curve (ROC) values greater than 0.8 for the test sets, indicating robust models with acceptable false positive and false negative prediction rates. Both MRP4 and BSEP inhibitor pharmacophore models were characterized by hydrophobic and hydrogen-bond acceptor features, albeit in distinct spatial arrangements; similar molecular features between MRP4 and BSEP inhibitors may partially explain why various drugs have affinity for both transporters. The Bayesian (BSEP, MRP4) and pharmacophore (MRP4, BSEP) models demonstrated significant classification accuracy and predictability.

DMD Fast Forward. Published on March 3, 2015 as DOI: 10.1124/dmd.114.062539
This article has not been copyedited and formatted. The final version may differ from this version.

Introduction

Drug-induced liver injury (DILI) is an important cause of drug toxicity and a major reason for withdrawal of drugs from the market (Abboud and Kaplowitz, 2007) or attrition of drug candidates in late development stages, which can be extremely costly. Unfortunately, current *in vitro* screens or *in vivo* preclinical studies cannot accurately predict the potential of compounds to cause hepatotoxicity. DILI remains a major concern in drug discovery and clinical development. This obstacle has necessitated a search for alternative technologies, such as computational approaches to decrease the risk of DILI-associated late-stage failures.

Despite extensive research, the underlying mechanisms of DILI are not well understood. However, it is clear that compound-related properties as well as individual patient characteristics affect the occurrence of DILI. Formation of reactive metabolites, mitochondrial impairment, and inhibition of canalicular bile acid transport mediated by the bile salt export pump (BSEP) (e.g. troglitazone, bosentan, erythromycin) (Stieger et al., 2000; Fattinger et al., 2001; Kostrubsky et al., 2003) are known risk factors for the development of DILI in humans. This has been substantiated by large scale *in vitro* screening studies revealing that drugs that cause cholestatic DILI have higher potencies as well as frequencies of BSEP inhibition compared to drugs that are not liver toxic or that cause hepatocellular DILI. (Morgan et al., 2010; Dawson et al., 2012) BSEP is located at the canalicular membrane of the hepatocyte where it is involved in the excretion of bile acids into bile under physiological conditions. (Noe et al., 2002) The importance of this protein in bile acid homeostasis is emphasized by the observation that mutations in the BSEP gene *ABCB11* have been associated with progressive familial intrahepatic cholestasis type 2 (PFIC 2). Although BSEP inhibition may explain bile acid-mediated DILI liability for a large proportion of compounds, a subset of hepatotoxic drugs remains that cannot be explained by BSEP inhibition alone.

DMD Fast Forward. Published on March 3, 2015 as DOI: 10.1124/dmd.114.062539
This article has not been copyedited and formatted. The final version may differ from this version.

In addition to canalicular BSEP, multidrug resistance protein 4 (MRP4) is a bile acid efflux protein localized at the basolateral membrane of hepatocytes. While hepatic expression is low under normal physiological conditions, MRP4 up-regulation has been demonstrated under cholestatic conditions. MRP4 is hypothesized to serve as a back-up system for bile acid efflux from hepatocytes into sinusoidal blood when the normal vectorial transport of bile acids from hepatocytes into bile is compromised. (Scheffer et al., 2002; Teng and Piquette-Miller, 2007; Gradhand et al., 2008; Chai et al., 2012) Recently, we screened 88 drugs (BSEP inhibitors and non-inhibitors) for inhibition of MRP4-mediated transport of the prototypical substrate [^{3}H]-dehydroepiandrosterone sulfate (DHEAS) and discovered potent MRP4 inhibition among cholestatic BSEP non-inhibitors. A statistically significant relationship was observed between the potency of MRP4 inhibition and the probability of cholestatic classification: for each 1% increase in MRP4 inhibition, the probability that a drug was cholestatic increased by 3.1%. Interestingly, many BSEP inhibitors also were MRP4 inhibitors. These data suggested that MRP4 inhibition may serve as a confounding factor in BSEP-mediated DILI, or in some cases lead to DILI in the absence of BSEP inhibition. Thus, MRP4 inhibition may be an additional risk factor for the development of cholestatic DILI.

The role of hepatic bile acid transport inhibition in the etiology of DILI emphasizes the urgent need to develop screening tools to accurately predict drug-bile acid transporter interactions. While *in vitro* membrane vesicle assays have been developed for BSEP and MRP4 screening, use of these assays early in drug development is time consuming, labor- and resource-intensive, and requires the physical availability of compounds (including metabolites) for testing. An alternative approach to *in vitro* testing is the use of computational models to predict drug-bile acid transporter interactions and aid in identifying transporter-associated DILI early in the drug

discovery process. For example, pharmacophore models have been used in ligand-based drug design to define the key structural characteristics that a molecule must possess in order to bind to the biological target (Ekins et al., 2012). Since models for BSEP have been reported recently (Pedersen et al., 2013; Ritschel et al., 2014), the aim of the current study was to develop a comprehensive model for MRP4 inhibition and evaluate its predictive ability. In addition, we developed Bayesian models to delineate molecular features underlying *both* MRP4 and BSEP inhibition. These *in silico* models were used to identify potential novel MRP4 inhibitors by virtual screening of an existing database, and to classify drugs as BSEP and MRP4 inhibitors in an effort to correlate these features with DILI incidence.

DMD Fast Forward. Published on March 3, 2015 as DOI: 10.1124/dmd.114.062539
This article has not been copyedited and formatted. The final version may differ from this version.

Materials and Methods

Dataset Composition. A dataset of 86 compounds derived from Köck and co-workers (Köck et al., 2014) was used for MRP4 inhibition modeling and a dataset of 257 compounds derived from Dawson et al. and Morgan et al. (Morgan et al., 2010; Dawson et al., 2012) was used for developing BSEP inhibition models. The compounds in these datasets were structurally diverse and from various therapeutic classes. They were classified as "cholestatic" or "non-cholestatic," according to DILI type reported in the literature. The compounds were further classified as "active" for the specified transporter if they had an $IC_{50} \leq 135$ μM for BSEP or a percent inhibition ≥ 21% compared to control at 100 μM for MRP4, otherwise they were classified as "inactive" against that transporter. The MRP4 classifications are based on findings by the Köck and co-workers that compounds that inhibit by at least 21% have a 50% chance of being cholestatic and the rationale for the BSEP classifications is to identify inhibitor compounds with both potent and moderate cholestatic risk, similar to Morgan et al. These classifications enable the identification of compounds that should be investigated further for their potential to cause cholestasis.

In addition to MRP4 and BSEP datasets, a database of 1,510 FDA-approved drugs was retrieved from DrugBank (http://www.drugbank.ca) (Law et al., 2014). The database was modified by removing ionic salts and large polymeric drugs and proteins, resulting in a catalogue of 1,488 drugs.

Training and Test Set Generation. The MRP4 and BSEP databases were separated into training and test sets by randomly dividing two-thirds of the compounds into the training set and the other third into the test set (Supplemental Table 1). Table 1 enumerates the number of

DMD Fast Forward. Published on March 3, 2015 as DOI: 10.1124/dmd.114.062539
This article has not been copyedited and formatted. The final version may differ from this version.

compounds in each set based on the respective transporter as well as the number of compounds that were classified as inhibitors and non-inhibitors.

The Bayesian modeling of MRP4 and BSEP used all the compounds in their respective training sets. In contrast, the pharmacophore models were developed using a subset of compounds from the training set. The MRP4 pharmacophore subset was based on clustering of the training set, which produced a subset of 9 compounds; analogously, the BSEP pharmacophore subset contained the strongest inhibitors, also producing a subset of 9 compounds. Details of subset generation and composition are explained further within the pharmacophore creation methods section.

The conformational models for pharmacophore creation were produced in LigandScout using the OMEGA conformer generator with the default best quality settings that produced a maximum of 500 conformations per molecule with an energy window of 10kcal/mol and RMS threshold difference of 0.4 to identify unique conformers. The common feature pharmacophore was generated using the default settings in LigandScout for ligand-based shared-feature pharmacophore creation with a feature tolerance scale of 1.0.

Principal Component Analysis (PCA) of Training, Test Set and DrugBank Molecules. The 3D molecular structures of 86 MRP4 inhibitors and non-inhibitors and the 257 BSEP inhibitors were obtained from PubChem (http://www.ncbi.nlm.nih.gov/pccompound). PCA plots of each transporters' training and test sets were produced in order to ensure that the two sets were representative of each other in terms of molecular descriptors. In addition, the training sets were compared to the modified DrugBank database (see above) to ensure that the training set was representative of currently approved drugs and had predictive power in that chemical space. The PCA plots were generated based on 8 molecular descriptors for each drug: ALogP, molecular

DMD Fast Forward. Published on March 3, 2015 as DOI: 10.1124/dmd.114.062539
This article has not been copyedited and formatted. The final version may differ from this version.

weight, number of hydrogen bond donors, number of hydrogen bond acceptors, number of rotatable bonds, number of rings, number of aromatic rings, and molecular fractional polar surface area. The molecular descriptors and PCA plots were generated within Discovery Studio 4.0 (DS 4.0; Accelrys, Inc. San Diego, CA). The two-dimensional plots (Fig. 2A-D) represent only the first two principal components of each comparison for visual clarity.

Common Feature Pharmacophore Generation and Validation. Ligand-based pharmacophores and conformational models were generated using LigandScout (version 3.12 build 20130912, Inte:Ligand, Vienna, Austria) [1,2] with default settings. The pharmacophore models for MRP4 inhibition were generated from a subset of drugs produced by clustering the training sets based on similarity of the pharmacophore radial distribution function. Drugs with similar pharmacophore features were clustered together and the most potent inhibitors of each cluster were included in the subset to train the pharmacophore model. The rationale of clustering is to generate a pharmacophore from a smaller training set while still maintaining the structural diversity of the original training set. If the common pharmacophore creation failed or produced a pharmacophore with less than 3 features, the drug that failed to align was removed from the training set. Of the 10 pharmacophores generated per training set, the pharmacophore that aligned with the most compounds in the training and test set, and had the highest score, was selected for further testing.

The MRP4 common feature pharmacophore was validated within LigandScout through virtually screening the test set for its ability to distinguish actives (i.e. drugs with ≥21% MRP4 inhibitory activity) from inactives (i.e. drugs with <21% MRP4 inhibitory activity). The conformational models of the test set were generated in an identical manner as the training set.

DMD Fast Forward. Published on March 3, 2015 as DOI: 10.1124/dmd.114.062539
This article has not been copyedited and formatted. The final version may differ from this version.

Drugs that aligned with all 3 pharmacophore features were predicted to be active MRP4 inhibitors.

The pharmacophore models for BSEP inhibition were generated from a subset of drugs from the BSEP training set that were the strongest inhibitors (<25 uM IC_{50}s) among the Morgan dataset (Morgan et al., 2010). This dataset was chosen because it contained the largest number of BSEP inhibitors. The clustering method utilized for the MRP4 inhibition pharmacophore was used initially; however, this resulted in a pharmacophore with poor predictive ability which is why the strongest inhibitors were used instead. The BSEP common feature pharmacophore was validated using the same methods as the MRP4 pharmacophore except that actives were drugs with an $IC_{50} \leq 135$ μM.

Building and Validation of Bayesian Models. Bayesian categorization involves simple and straightforward probabilistic classification by evaluating the frequency of structural features associated with a hypothesis of interest (Xia et al., 2004). The protocol "Create Bayesian Model" in DS4.0 was applied for model generation with the number of bins set to 10. In addition to 7 molecular descriptors, 'extended-connectivity fingerprints maximum diameter 6' (ECFP_6) and 'functional-class fingerprints maximum diameter 6' (FCFP_6) (Rogers et al., 2005) were calculated for all compounds. ECFP and FCFP differ such that, for example, a chlorine atom and a bromine atom, which are substituents in the same position on an aromatic ring, would be differentiated as different fingerprints with ECFP but not with FCFP. The models were built by using combinations of iterative sets of varying descriptors and cutoff values. Bayesian models were validated with 10-fold cross-validation-based 'receiver operator curve' area under the curve (XV ROC AUC) (Zweig and Campbell, 1993) associated with training set compounds. The predictive capacity of Bayesian models was validated with the same test set described for

DMD Fast Forward. Published on March 3, 2015 as DOI: 10.1124/dmd.114.062539
This article has not been copyedited and formatted. The final version may differ from this version.

pharmacophore generation above. The activities of the test set compounds were predicted by the "Calculate Molecular Properties" protocol in DS4.0.

Evaluation of Model Performance. The Matthews correlation coefficient (MCC) was used to determine the relative predictive ability of the pharmacophore and Bayesian models. MCC ranges from –1 (no correlation) to +1 (full correlation) and is calculated as follows:

$$MCC = \frac{TP \times TN - FP \times FN}{\sqrt{(TP+FP)(TP+FN)(TN+FP)(TN+FN)}} \qquad \text{(Eq.1)}$$

where TP= number of true positives, FP=number of false positives, TN=number of true negatives, and FN=number of false negatives. Positive predictive value = TP/(TP+FP), sensitivity = TP/(TP+FN), and specificity = TN/(TN+FP).

The ROC curve is another method of evaluating models. It is a 2D plot that graphs the sensitivity of a model, its true positive rate, versus the reverse percentage of the specificity of the model, its false positive rate, by the ranked order of the pharmacophore-fit scores. One of the abilities of the ROC curve is the use of the area under the curve (AUC) when comparing the ability of different models to correctly classify true positives above false positives. Starting from the bottom left corner, the graph plots the percentage of the actives in the test set properly classified as active, which is defined as the sensitivity or true positive rate, versus the percentage of the inactives improperly classified as active, which is defined as the reverse specificity or false positive rate. In addition to the AUC, the ROC can be used to set a score cutoff which optimizes the tradeoff between sensitivity and specificity.

DMD Fast Forward. Published on March 3, 2015 as DOI: 10.1124/dmd.114.062539
This article has not been copyedited and formatted. The final version may differ from this version.

RESULTS

Characteristics of the data set. The MRP4 inhibitor data were obtained from data previously generated in our laboratories (Köck et al., 2014) and the BSEP inhibitor data were compiled from two high-throughput screening studies (Morgan et al., 2010; Dawson et al., 2012). The BSEP studies were selected due to the large number of screened compounds from various therapeutic areas (Supplemental Table S1). Venn diagrams reveal the composition of the MRP4 inhibitor dataset contrasted with the BSEP data from Morgan and colleagues to illustrate compounds in the dataset that uniquely inhibit MRP4 or BSEP as well as compounds that inhibit both transporters simultaneously (Fig. 1). These diagrams demonstrate that most of the previously identified BSEP inhibitors tested by our laboratories were also MRP4 inhibitors (Fig. 1A). Among cholestatic compounds, most were dual BSEP and MRP4 inhibitors or MRP4-only inhibitors; only one BSEP-only inhibitor had been identified as cholestatic (Fig. 1B).

Structure Generation and Validation. The PCA plot is a useful tool to predict potential outliers by assessing similarity among training and test set compounds (Khandelwal et al., 2007). For the MRP4 dataset, PCA of 86 training and test set drugs with at least three principal components was performed based on 8 descriptors. There were 57 compounds from the training set and 29 from the test set. The first and second components accounted for 36.6% and 27.2% of the total variance. For the BSEP dataset, PCA of 257 compounds compared 171 and 86 compounds in the training and test sets, respectively. The first and second components accounted for 39.1% and 34.4% of the total variance, indicating that these components represented the majority of overall descriptor space occupied by the molecules. Figures 2A-B demonstrate that the test set drugs accommodate similar space compared with the training set compounds for their respective transporter. PCA plots of compounds in the training sets are overlaid on a PCA plot of DrugBank

drugs in Figures 2C-D, illustrating that training set compounds cover most of the descriptor space occupied by the compounds featured in the DrugBank database.

Building and Validation of Bayesian Models. Bayesian models for MRP4 inhibition were developed with a training set of 57 MRP4 inhibitors and non-inhibitors and the Bayesian models for BSEP inhibition were developed with a training set of 171 inhibitors and non-inhibitors. Eight structural descriptors as well as structural extended-connectivity or functional-class fingerprints (ECFP_6 or FCFP_6, see Methods) were incorporated for model development. Four Bayesian models were generated for MRP4 and BSEP inhibitors and non-inhibitors based on specified atom-type (ECFP) and functional class (FCFP) 2-dimensional substructure fingerprints.

The predictive performance of Bayesian models was evaluated by XV ROC AUC based on 10-fold cross-validation of training set compounds. XV ROC AUC reflects the relationship between sensitivity and specificity, ranging from 0 to 1, with a higher number indicating a better model (Zweig and Campbell, 1993; Obuchowski and Lieber, 1998). The Bayesian models also were validated with their respective test set, consisting of 29 drugs for the MRP4 model and 86 drugs for the BSEP model. Their predicted performance was established by sensitivity (SE), specificity (SP), overall prediction accuracy (Q) and Matthew's correlation coefficients (MCC values; a measure of the quality of binary classifications) calculated from the empirical true positive (TP), true negative (TN), false positive (FP), and false negative (FN) values (Ung et al., 2007; Khandelwal et al., 2008) (Table 2).

Table 2 shows the AUCs of Bayesian models based on the 10-fold cross-validation with training set compounds. AUC values range between 0 and 1, with 0.5 indicating 50% correct prediction and 1 indicating a perfect match between observed and predicted data (Fawcett, 2006). The AUC values associated with the four individual models indicated good internal

consistency and prediction accuracy. While both the MRP4 inhibitor and the BSEP inhibitor Bayesian classification had similar ROC AUC scores for both the internal, leave-one-out cross-validation, and the external test set validation, the sensitivity and specificity varied more between the models. The MRP4 inhibitor models had significantly lower sensitivity, especially the MRP4 ECFP model, compared to the BSEP inhibitor models, but the trade-off was a higher specificity, minimizing false positives. Bayesian classification modeling of BSEP inhibitors resulted in more predictive models as demonstrated by their relatively higher Matthews' correlation coefficient compared to MRP4 inhibitor models, which could be due to the larger size of the training set (171 BSEP compounds vs. 59 MRP4 compounds). In addition to the external validation performed here, the BSEP Bayesian FCFP model was used to predict the classification of 5 strong inhibitors and 5 non-inhibitors from previous screen for BSEP inhibitors (Pedersen et al., 2013). The model was able to correctly classify nine of the ten compounds, only incorrectly classifying MK571 as a non-inhibitor.

Fingerprints can be defined as molecular fragments that characterize the structural features of drug molecules. Figure 3 and 4 displays the five most predictive structural fragments for both favorable and unfavorable inhibitory activity against MRP4 and BSEP using FCFP_6 fingerprints. Supplemental figure S2 contains an expanded figure of structural fragments favorable and unfavorable for inhibition of MRP4 and BSEP using both FCFP_6 and ECFP_6 fingerprints. Structural elements depicted in Figure 3 and 4 were identified in inhibitors and non-inhibitors amongst training set compounds, respectively. Oxygen atoms tended to be predictive of favorable inhibitory activity for both MRP4 and BSEP, however, negatively ionized oxygen atoms frequently occurred in the MRP4 model but not in the BSEP model even though both are considered anion transporters. This is in agreement with the study by Pedersen and

colleagues (Pedersen et al., 2013), who reported that BSEP substrates tend to be anionic but inhibitors were more likely to be neutral at physiological pH. Accordingly, positively charged secondary and tertiary amines frequently occur among the MRP4 fingerprints associated with non-inhibition. Thus, the identified fingerprints could be helpful in distinguishing inhibitors and non-inhibitors of MRP4 amongst novel compounds.

MRP4 Pharmacophore Development. The MRP4 training set of 57 drugs was imported into LigandScout 3.12 and clustered according to pharmacophore radial distribution function-code similarity with the maximum conformations set to 3 and the cluster distance set to 0.5. This algorithm clusters compounds that have similar individual 3D pharmacophore characteristics.

The following 9 drugs that represent the strongest inhibitors in their respective cluster were used to generate MRP4 inhibition pharmacophores: nitrenedipine, sulindac, sorafenib, clobetasol propionate, benzbromarone, glafenine, furosemide, finasteride, and simvastatin. The remaining 77 compounds not selected for the training set were moved to the test set for pharmacophore validation. The ligand-based common feature pharmacophore produced from the 9 compounds had 2 hydrophobic features and a hydrogen bond acceptor feature (Fig 5A). The two hydrophobic features were 5.01Å apart, while the hydrogen bond acceptor was 4.81Å from the neighboring hydrophobic feature, and 8.86Å from the distal hydrophobic group. All 9 drugs in the training set aligned with all 3 pharmacophore features. Two representative compounds were aligned to the pharmacophore to illustrate scale and similarity in how the molecules align with the respective molecular features comprising the pharmacophore (Fig 5B). These compounds were chosen because their steroid backbone renders them particularly rigid, increasing the likelihood that the representative conformer is close to its bioactive conformation; additionally, they contain few atoms that can engage in intermolecular interactions, which further confirms

DMD Fast Forward. Published on March 3, 2015 as DOI: 10.1124/dmd.114.062539
This article has not been copyedited and formatted. The final version may differ from this version.

that these are the requisite features for MRP4 recognition. Exclusion volumes, i.e. spheres that cannot be occupied and represent steric hindrance, were generated initially using the non-inhibitors in the 57 compound training set; however, consideration of exclusion volumes rendered the models more likely to incorrectly classify MRP4 inhibitors as non-inhibitors during external validation and were subsequently omitted during database screening.

Quantitative validation of the MRP4 pharmacophore model. The MRP4 pharmacophore model was able to correctly classify 30 of the 42 actives in the test set and 22 of the 35 inactives, featuring model sensitivity of 71.4% and specificity of 62.8%. The area under the receiver operating characteristic curve was 0.70, which is considered a fair quality model (Fig 6). Based on the virtual screening results from the external test set validation, the model has its highest positive predictive value, the number of true positives over the sum of true and false positives, at a pharmacophore-fit score cutoff of 37.75. The positive predictive value of the model at this cutoff is 0.826, selecting 19 true positives, 45.2% of total actives in the set, but only 4 false positives, 11.4% of total inactives in the set. The pharmacophore-fit score cutoffs allow for selecting drugs with a higher likelihood of being classified correctly beyond those which align to the pharmacophore within the tolerance of the features.

The inactives that were incorrectly classified included dexamethasone, naloxone, clopamide, vinblastine, tolbutamide, probenecid, indinavir, flupirtine, chorpropamide, alprenolol, chlorpheniramine, fluorescein, and timolol. Interestingly, the false positive with the highest pharmacophore-fit score was dexamethasone, a glucocorticoid that had no significant inhibitory activity (5 ± 34%). This compound was aligned with clobetasol propionate, another glucocorticoid included in the 9 training set compounds, which was a strong inhibitor (101 ± 23%) (Fig 7).

DMD Fast Forward. Published on March 3, 2015 as DOI: 10.1124/dmd.114.062539
This article has not been copyedited and formatted. The final version may differ from this version.

As can be seen in Fig. 7, clobetasol propionate (orange) and dexamethasone (gray) have a high degree of structural similarity. From this observation, molecular properties that could be mediating the significant difference in inhibitory activity were investigated. The molecular property that exhibited the most significant difference was calculated LogP which is 4.18 for clobetasol propionate and 1.68 for dexamethasone, rendering clobetasol propionate a more hydrophobic compound. The difference in calculated LogP values was evaluated for all 87 compounds tested by Köck and co-workers; actives trended towards higher LogP values than inactives. A Pearson correlation coefficient for the calculated LogP and a compound considered active (≥21% MRP4 inhibition) was 0.634 and the correlation coefficient for the percent MRP4 inhibition and calculated LogP was 0.508. Figure 8 represents a box plot of the calculated LogP values for the compounds classified as inactives and actives; the mean and median of the inactives' calculated LogP values were 0.38 and 0.69, respectively, and the actives' calculated LogP values were 3.64 and 3.84, respectively. It is interesting to note that numerous sulfonamides or sulfamides, such as clopamide, tolbutamide, probenecid, and chlorpropamide were classified as false positives. These molecules may either be a poor match to the models, or their features are incorrectly parameterized within the Bayesian and pharmacophore modeling algorithms.

The actives that were not properly classified as active by the model included 19-norethindrone, clozapine, desipramine, diphenhydramine, etoposide, maprotiline, nitrofurantoin, nortriptyline, oxybutynin, praziquantel, promethazine, and ticlodipine. Eight of these 12 drugs have similar structures containing an amine group, which is predicted to be positively ionized at physiological pH; in addition, six of these drugs contain two aromatic rings whose distance is comparable to the distance observed between the two hydrophobic features in the MRP4 model. Compounds

that fall into this category are clozapine, desipramine, diphenhydramine, maprotiline, nortriptyline, and promethazine. Oxybutynin and ticlodipine contain an amine predicted to be positively charged, but they have only one aromatic group. Nitrofurantoin is a compound that continually failed to match any structural similarity search to other known inhibitors; therefore, we speculate that it is binding in a different manner than any of the other inhibitors, perhaps at an allosteric site of the transporter.

Qualitative Validation of the MRP4 Inhibitor Model. In addition to the quantitative validation from virtually screening the test set, two compounds that qualitatively strengthen confidence in the model are DHEAS, the substrate used to generate the data, and felbinac, a potent MRP4 inhibitor from a separate screening of MRP4 inhibitors (Morgan et al., 2013). DHEAS was not included in either the training set or the test set, but the MRP4 pharmacophore model would be expected to align to the substrate that was used experimentally to generate the inhibition data. Figure 9A depicts how the two methyl groups on DHEAS align to the hydrophobic features in the pharmacophore and one of the oxygen atoms from the sulfate group aligns with the hydrogen bond acceptor feature. The alignment of the pharmacophore model to DHEAS is of particular interest because of its structural rigidity due to the steroid backbone structure. The only significant intramolecular motion that DHEAS can undergo is the rotation of the sulfate group. In addition to its rigidity, DHEAS contains few atoms that can participate in intermolecular interactions. From the DHEAS pharmacophore (Fig 9B), it appears that the two methyl groups can participate in hydrophobic interactions, while the ketone can be a hydrogen bond acceptor, and all the oxygen atoms in the sulfate group, which is negatively ionized at physiological pH, can act as hydrogen bond acceptors.

Felbinac is of interest for the same reasons as DHEAS, namely its structural rigidity and minimal possible intermolecular interactions. In addition, felbinac is a potent inhibitor of MRP4-mediated transport of β-estradiol 17-(β-D-glucuronide) with an IC_{50} of 8.2 uM. (17) Felbinac aligns well with the MRP4 pharmacophore model and, as shown in Figure 9D, engages in only a limited number of intermolecular interactions; both hydrophobic and aromatic interactions with the phenyl groups in the biphenyl compound, and the oxygen atoms of the negatively ionized carboxylate group, are able to act as hydrogen bond acceptors. The two phenyl groups are locked rigidly on perpendicular planes and, therefore, only the carboxylate group is able to rotate.

LogP Filtering Improves Model Specificity. The MRP4 pharmacophore model's specificity can be significantly improved if the test set were to be filtered after screening with a calculated LogP cutoff of 2.92, which corresponds to the start of the lower quartile of the actives. The sensitivity would decrease to 52.38% (22 true actives of 42 total actives) but the specificity would increase to 91.43% (3 false actives of 35 total inactives). This marked improvement in specificity demonstrates the significant influence LogP plays in MRP4 inhibition.

BSEP Inhibitor Pharmacophore Development and Validation. The BSEP inhibitor pharmacophore was produced with a subset of drugs from the training set that represented the nine strongest BSEP inhibitors according to Morgan and co-workers that were also tested for MRP4 inhibition by our group previously. This subset included: nitrenedipine, fenofibrate, ritonavir, pioglitazone, rosiglitazone, valinomycin, simvastatin, benzbromarone, and lopinavir. The common feature pharmacophore produced with this set of nine compounds had three features: two hydrophobic features and one hydrogen bond acceptor (Supplemental Figure S1). This is similar to the MRP4 pharmacophore, which may explain the high degree of inhibition

overlap, however, the distances between the features were different. The distance between the two hydrophobic features was 6.29 Å, the hydrogen bond acceptor and the proximal hydrophobic feature was 4.67 Å, and the hydrogen bond acceptor and the distal hydrophobic feature was 6.69 Å. All nine drugs that were used to train the pharmacophore hit all three features.

The BSEP inhibitor pharmacophore was validated by virtual screening of the test set and the model correctly classified 46 of the 56 inhibitors and incorrectly classified 120 of the 191 non-inhibitors. The model selectivity was 82.7% but the specificity was 37.2%. The poor model specificity is partly due to the higher proportion of non-inhibitors to inhibitors in the test set (191 vs. 56) but also indicative of the difficulty of modeling BSEP through a pharmacophore approach.

DISCUSSION

A ligand-based pharmacophore and Bayesian modeling approach is presented here, describing the molecular properties and chemical features necessary for human MRP4 and BSEP interaction. Since these transport proteins have been associated with DILI, these models may be useful in predicting DILI liability of novel compounds. The models were developed from our laboratories' previous work and data from other groups. An advantage of Bayesian classification modeling is the ability to easily interpret how the model weighs the various molecular properties, and which molecular properties are most predictive for classification. The Bayesian classification model was developed by creating up to 11 bins for each molecular property. For discrete properties such as the number of rings or the hydrogen-bond acceptor atoms, all the compounds with the same value were put into the same bin; for continuous properties such as molecular weight or ALogP, a bin was assigned a value range and all the compounds that fell within that range were put into that bin. The ranges for binning continuous values were created

such that the number of compounds in each bin was evenly distributed. A normalized probability was then calculated for each bin according to the fraction of compounds in the bin that were active, i.e. if all the compounds in a bin were active, that bin was assigned a higher probability. The probability was normalized by adjusting for bins with few compounds. A Bayesian score was then calculated by summing the normalized probabilities of all the bins to which a compound was assigned.

By inspecting the normalized probabilities of individual bins, the molecular properties that contain bins with high probabilities indicate molecular properties that are well correlated with either inhibition or non-inhibition. For example, with the MRP4 model, a trend was observed with a higher ALogP correlating to MRP4 inhibition (14 of 15 drugs with an ALogP of 3.8 or higher were inhibitors while only 2 of 12 drugs with a ALogP of 0.94 or lower were inhibitors). A trend also was observed with large molecular weight drugs more likely to inhibit MRP4 compared to smaller drugs (23 of 25 drugs with molecular weight ≥356 Da). It should again be noted that the value range of a bin, for molecular properties that are continuous, is a result of evenly dividing the ordered drugs into 11 bins. In addition to those continuous properties, 23 of 25 drugs with 3 or 4 rings were inhibitors compared to 1 of 9 compounds with 0 or 1 ring.

Compared to the MRP4 Bayesian model, the BSEP Bayesian model was more predictive of negative properties, thus predicting more non-inhibitors than inhibitors. This is likely due to the fact that the training set contained more non-inhibitors relative to inhibitors compared to the MRP4 training set. For the BSEP model, only 7 of 90 drugs with a molecular weight less than 337 Da were inhibitors. Correspondingly, only 11 of 90 compounds with 4 or fewer rotatable bonds were inhibitors and, similar to the MRP4 model, only 3 of 72 drugs with an ALogP of 2.03 or lower were inhibitors.

Potential biological implications of the association between high calculated LogP values and MRP4 inhibition were considered. These data lead to speculation that molecules must partition first into the bilayer to be an inhibitor for MRP4, or that higher LogP values correspond with increased hydrophobic interactions within the protein environment, thus rendering these molecules stronger competitive inhibitors.

It is worth mentioning that these computational models are based on data collected from membrane vesicle assays and this *in vitro* system could have an influence on experimental transport inhibition results. The methods generally involve short incubation periods with the test compounds in which the degree of partitioning of the test compound into the membrane of the vesicles could be in flux. If the test compound exerts its inhibition while imbedded in the membrane, this could cause a skew in the data in which compounds with higher LogP values have a higher rate of partitioning into the membrane than those with lower LogP values.(Nagar and Korzekwa, 2012)

Comparison to Previous Models. Previous studies identified important molecular features for BSEP inhibition (Pedersen et al., 2013) and pharmacophore models have been proposed for BSEP (Ritschel et al., 2014) and MRP4 (Fukuda et al., 2013). While there was good corroboration between the important molecular features, there were several notable differences between the pharmacophores previously reported and those developed here, which can be ascribed primarily to differences in the training sets used to generate the pharmacophores.

Molecular properties that were reported previously to have a statistically significant difference between strong BSEP inhibition (>50% inhibition) and non-inhibitors were $LogD_{7.4}$, molecular weight, saturated nonpolar surface area, LogP, number of rotatable bonds, unsaturated nonpolar

surface area, number of hydrogen-bond acceptors, and net charge at pH 7.4. The molecular properties that remain statistically significant for weak inhibitors (27-50% inhibition) and non-inhibitors were only molecular weight and saturated nonpolar surface area. In comparison, our best Bayesian BSEP model (FCFP_6) ranked the top four feature bins based on their normalized probability in descending order: molecular weight, FCFP_6 fingerprint, number of rotatable bonds, and ALogP. However, since a compound can have only one value for a molecular property but multiple fingerprints, the fingerprints tend to be the predominate factor influencing the final Bayesian score for a compound. The pharmacophore model for BSEP is also in agreement with these previously reported molecular properties since they consisted of 2 hydrophobic features and a hydrogen-bond accepting feature. The hydrophobic features were associated with nonpolar surface area and high LogP while the hydrogen-bond accepting feature was associated with the number of hydrogen bond acceptors correlated with inhibition. The presence of only one hydrogen-bond accepting features in the pharmacophore model, however, suggests that a large number is not essential for inhibition, but could provide more opportunities for hydrogen bonding in the correct spatial arrangement.

Two common feature MRP4 pharmacophores were reported previously in the same paper; one, based on five protease inhibitors (PI) and, the other based on a more diverse set of ten drugs that were inhibitors based on literature reports. The pharmacophore based on five PIs resulted in a pharmacophore with four hydrogen bond acceptors (HBA), one hydrogen bond donor (HBD), and three hydrophobic features, and the pharmacophore based on ten drugs resulted in two HBAs and a hydrophobic feature. The PI-based pharmacophore featured a large number of features due to the small number of compounds in the training set and their high degree of structural similarity while the pharmacophore based on ten diverse compounds was based on the findings

from multiple labs. The MRP4 pharmacophore we developed is more appropriate for predicting potential MRP4 inhibitors in order to identify the cholestatic potential of compounds because it was based on data from a single laboratory utilizing one assay, was developed based on a diverse set of compounds, and contained a large number of inhibitors.

The other recently reported BSEP pharmacophore (Ritschel et al., 2014) was trained using five compounds of limited structural diversity, and resulted in a pharmacophore that had eight features; four hydrophobic features and two HBAs that had an associated vector feature. The authors found the pharmacophore too stringent so they modified it by making only four hydrophobic features in the core of the pharmacophore essential. The advantage of the BSEP pharmacophore presented in this paper is that it is derived from pharmaceuticals instead of a chemical library and developed with more diverse compounds, which results in a pharmacophore with fewer features, but one more equipped to deal with a larger chemical space. The BSEP pharmacophore reported in this paper, however, is able to align with the hydrophobic and hydrogen bond accepting features of the previously reported BSEP pharmacophore. This suggests that the pharmacophore reported in this paper may be convergent with previously reported pharmacophore, although less stringent.

In conclusion, ongoing studies will utilize these models in an ensemble fashion against drugs that are predicted to be MRP4 or BSEP inhibitors in order to further validate the models. These models, when used in combination, may aid in the *a priori* identification of potential cholestasis-inducing compounds during the early stages of drug development.

Authorship Contributions

Participated in research design: Brouwer, Köck, Swaan, Welch

Conducted experiments: Welch

Performed data analysis: Swaan, Welch

Wrote or contributed to the writing of the manuscript: Welch, Köck, Urban, Brouwer, Swaan

References

Abboud G and Kaplowitz N (2007) Drug-induced liver injury. *Drug safety : an international journal of medical toxicology and drug experience* **30:**277-294.

Chai J, He Y, Cai SY, Jiang Z, Wang H, Li Q, Chen L, Peng Z, He X, Wu X, Xiao T, Wang R, Boyer JL, and Chen W (2012) Elevated hepatic multidrug resistance-associated protein 3/ATP-binding cassette subfamily C 3 expression in human obstructive cholestasis is mediated through tumor necrosis factor alpha and c-Jun NH2-terminal kinase/stress-activated protein kinase-signaling pathway. *Hepatology* **55:**1485-1494.

Dawson S, Stahl S, Paul N, Barber J, and Kenna JG (2012) In vitro inhibition of the bile salt export pump correlates with risk of cholestatic drug-induced liver injury in humans. *Drug Metabolism and Disposition* **40:**130-138.

Ekins S, Polli JE, Swaan PW, and Wright SH (2012) Computational modeling to accelerate the identification of substrates and inhibitors for transporters that affect drug disposition. *Clin Pharmacol Ther* **92:**661-665.

Fattinger K, Funk C, Pantze M, Weber C, Reichen J, Stieger B, and Meier PJ (2001) The endothelin antagonist bosentan inhibits the canalicular bile salt export pump: a potential mechanism for hepatic adverse reactions. *Clin Pharmacol Ther* **69:**223-231.

Fawcett T (2006) An introduction to ROC analysis. *Pattern Recogn Lett* **27:**861-874.

Fukuda Y, Takenaka K, Sparreboom A, Cheepala SB, Wu C-P, Ekins S, Ambudkar SV, and Schuetz JD (2013) Human immunodeficiency virus protease inhibitors interact with ATP binding cassette transporter 4/multidrug resistance protein 4: a basis for unanticipated enhanced cytotoxicity. *Molecular pharmacology* **84:**361-371.

Gradhand U, Lang T, Schaeffeler E, Glaeser H, Tegude H, Klein K, Fritz P, Jedlitschky G, Kroemer HK, Bachmakov I, Anwald B, Kerb R, Zanger UM, Eichelbaum M, Schwab M, and Fromm MF (2008) Variability in human hepatic MRP4 expression: influence of cholestasis and genotype. *The pharmacogenomics journal* **8:**42-52.

Khandelwal A, Bahadduri PM, Chang C, Polli JE, Swaan PW, and Ekins S (2007) Computational models to assign biopharmaceutics drug disposition classification from molecular structure. *Pharm Res* **24:**2249-2262.

Khandelwal A, Krasowski MD, Reschly EJ, Sinz MW, Swaan PW, and Ekins S (2008) Machine learning methods and docking for predicting human pregnane X receptor activation. *Chem Res Toxicol* **21:**1457-1467.

Kostrubsky VE, Strom SC, Hanson J, Urda E, Rose K, Burliegh J, Zocharski P, Cai H, Sinclair JF, and Sahi J (2003) Evaluation of hepatotoxic potential of drugs by inhibition of bile-acid transport in cultured primary human hepatocytes and intact rats. *Toxicological sciences : an official journal of the Society of Toxicology* **76:**220-228.

Köck K, Ferslew BC, Netterberg I, Yang K, Urban TJ, Swaan PW, Stewart PW, and Brouwer KL (2014) Risk Factors for Development of Cholestatic Drug-Induced Liver Injury: Inhibition of Hepatic Basolateral Bile Acid Transporters Multidrug Resistance-Associated Proteins 3 and 4. *Drug Metabolism and Disposition* **42:**665-674.

Law V, Knox C, Djoumbou Y, Jewison T, Guo AC, Liu Y, Maciejewski A, Arndt D, Wilson M, and Neveu V (2014) DrugBank 4.0: shedding new light on drug metabolism. *Nucleic acids research* **42:**D1091-D1097.

Morgan RE, Trauner M, van Staden CJ, Lee PH, Ramachandran B, Eschenberg M, Afshari CA, Qualls CW, Jr., Lightfoot-Dunn R, and Hamadeh HK (2010) Interference with bile salt export pump function

is a susceptibility factor for human liver injury in drug development. *Toxicological sciences : an official journal of the Society of Toxicology* **118:**485-500.

Morgan RE, van Staden CJ, Chen Y, Kalyanaraman N, Kalanzi J, Dunn RT, Afshari CA, and Hamadeh HK (2013) A multifactorial approach to hepatobiliary transporter assessment enables improved therapeutic compound development. *Toxicological Sciences* **136:**216-241.

Nagar S and Korzekwa K (2012) Commentary: Nonspecific Protein Binding versus Membrane Partitioning: It Is Not Just Semantics. *Drug Metabolism and Disposition* **40:**1649-1652.

Noe J, Stieger B, and Meier PJ (2002) Functional expression of the canalicular bile salt export pump of human liver. *Gastroenterology* **123:**1659-1666.

Obuchowski NA and Lieber ML (1998) Confidence intervals for the receiver operating characteristic area in studies with small samples. *Acad Radiol* **5:**561-571.

Pedersen JM, Matsson P, Bergström CA, Hoogstraate J, Norén A, LeCluyse EL, and Artursson P (2013) Early identification of clinically relevant drug interactions with the human bile salt export pump (BSEP/ABCB11). *toxicological sciences* **136:**328-343.

Ritschel T, Hermans S, Schreures M, van den Heuvel J, Koenderink JB, Greupink R, and Russel F (2014) In silico identification and in vitro validation of potential cholestatic compounds through 3D ligand-based pharmacophore modeling of BSEP inhibitors. *Chemical research in toxicology*.

Rogers D, Brown RD, and Hahn M (2005) Using extended-connectivity fingerprints with Laplacian-modified Bayesian analysis in high-throughput screening follow-up. *J Biomol Screen* **10:**682-686.

Scheffer GL, Kool M, de Haas M, de Vree JM, Pijnenborg AC, Bosman DK, Elferink RP, van der Valk P, Borst P, and Scheper RJ (2002) Tissue distribution and induction of human multidrug resistant protein 3. *Laboratory investigation; a journal of technical methods and pathology* **82:**193-201.

Stieger B, Fattinger K, Madon J, Kullak-Ublick GA, and Meier PJ (2000) Drug- and estrogen-induced cholestasis through inhibition of the hepatocellular bile salt export pump (Bsep) of rat liver. *Gastroenterology* **118:**422-430.

Teng S and Piquette-Miller M (2007) Hepatoprotective role of PXR activation and MRP3 in cholic acid-induced cholestasis. *British journal of pharmacology* **151:**367-376.

Ung CY, Li H, Yap CW, and Chen YZ (2007) In silico prediction of pregnane X receptor activators by machine learning approaches. *Mol Pharmacol* **71:**158-168.

Xia X, Maliski EG, Gallant P, and Rogers D (2004) Classification of kinase inhibitors using a Bayesian model. *J Med Chem* **47:**4463-4470.

Zweig MH and Campbell G (1993) Receiver-operating characteristic (ROC) plots: a fundamental evaluation tool in clinical medicine. *Clin Chem* **39:**561-577.

Footnotes

Financial support: This work was supported by the National Institutes of General Medical Sciences and Digestive Diseases & Kidney of the National Institutes of Health [Grant R01 GM041935, R01 DK61425, U01DK065201, and an NIGMS Collaborative Science Supplement]; and by Deutsche Forschungsgemeinschaft [Grant Ko4186/1-1]. The content is solely the responsibility of the authors and does not necessarily represent the official views of the National Institutes of Health.

DMD Fast Forward. Published on March 3, 2015 as DOI: 10.1124/dmd.114.062539
This article has not been copyedited and formatted. The final version may differ from this version.

Figure Legends

Figure 1. A. Classification of the inhibitors used in development of the MRP4 models. Forty-five drugs were MRP4 inhibitors *only* and 31 drugs were BSEP inhibitors *only*, whereas 26 molecules inhibited both MRP4 *and* BSEP. **B.** Of the compounds in ***A***, 14 MRP4 inhibitors were cholestatic, whereas only one BSEP inhibitor was identified as a cholestatic drug. Of the 26 compounds classified as both MRP4 and BSEP inhibitors, 15 (58%) were clinically identified as cholestatic.

Figure 2. A. MRP4: Principal component analysis (PCA) of the training and test set compounds (257 total) were selected such that they occupy similar areas of the PCA plot. The PCA among training and test set compounds was generated with the following properties: ALogP, molecular weight, molecular fractional polar surface area, number of rings, aromatic rings, rotatable bonds, hydrogen bond acceptors and hydrogen bond donors. The first principal component explains 0.366 of total variance and the second principal component explains 0.272 of total variance; when combined these explain 0.638 of the total variance. The principal components are linear combinations of original descriptors. The dominate descriptors in the principal components are determined by the product of the descriptor coefficient while accounting for the magnitude of the descriptor. The first principal component is dominated by molecular weight, number of hydrogen bond acceptors, and number of rotatable bonds. The second principal component is dominated by molecular fractional polar surface area.

Component 1: = -3.8514 + 0.17609 * [ALogP] + 0.0029942 * [Molecular_Weight] + 0.19241 * [Num_H_Donors] + 0.12966 * [Num_H_Acceptors] + 0.11058 * [Num_RotatableBonds] + 0.21601 * [Num_Rings] + 0.26649 * [Num_AromaticRings] - 0.91018 * [Molecular_FractionalPolarSurfaceArea]
Component 2: = -0.91763 - 0.22028 * [ALogP] + 0.00060715 * [Molecular_Weight] + 0.30038 * [Num_H_Donors] + 0.1113 * [Num_H_Acceptors] + 0.0097512 * [Num_RotatableBonds] - 0.15452 * [Num_Rings] - 0.34347 * [Num_AromaticRings] + 4.3042 * [Molecular_FractionalPolarSurfaceArea]

DMD Fast Forward. Published on March 3, 2015 as DOI: 10.1124/dmd.114.062539
This article has not been copyedited and formatted. The final version may differ from this version.

B. BSEP: PCA analysis of the training and test sets. The first and second principal components accounted for 0.391 and 0.344 of total variance, respectively. Together they explain 0.735 of the total variance. The first principal component (*x*-axis) is governed by the number of hydrogen bond donors/acceptors and number of rings, whereas the second principal component (*y*-axis) is governed by lipophilicity and the number of aromatic rings. Both principal components are strongly influenced by fractional polar surface area.

Component 1: = -4.0005 + 0.035399 * [ALogP] + 0.0031256 * [Molecular_Weight] + 0.16608 * [Num_H_Donors] + 0.14138 * [Num_H_Acceptors] + 0.11881 * [Num_RotatableBonds] + 0.23456 * [Num_Rings] + 0.23836 * [Num_AromaticRings] + 0.48987 * [Molecular_FractionalPolarSurfaceArea]
Component 2: = -0.12988 + 0.2367 * [ALogP] + 0.00047919 * [Molecular_Weight] - 0.20734 * [Num_H_Donors] - 7.2971e-002 * [Num_H_Acceptors] + 0.019248 * [Num_RotatableBonds] + 0.16242 * [Num_Rings] + 0.31811 * [Num_AromaticRings] - 3.6221 * [Molecular_FractionalPolarSurfaceArea]

PCA analysis comparing the training set of MRP4 (**C**) and BSEP (**D**) to the DrugBank database of FDA-approved drugs.

Figure 3. Favorable and unfavorable molecular features for interactions with MRP4. Each feature is a fragment-like fingerprint, up to 6 bond lengths in diameter, which occurs within the larger parent molecule. The squiggle and asterisks indicate that the bond extends further but does not specify the atom type. The favorable features or "good" features are labeled G1-G5 and the unfavorable features or "bad" features are labeled B1-B5. A feature is considered good if it frequently occurs within compounds that were classified as inhibitors and bad if it frequently occurs in compounds that are non-inhibitors. The large integer after the colon is the unique hash identifier for the shown fingerprint. The Bayesian score is the normalized probability assigned to that feature.

Figure 4. Favorable and unfavorable molecular features for interactions with BSEP.

Figure 5. Pharmacophore model of inhibitors of MRP4-mediated transport of DHEAS. **A.** The pharmacophore model with the measured distances between the 3 features. **B.** The pharmacophore model aligned with chemical groups of two drugs from the training set, clobetasol propionate (orange) and finasteride (lavender). Yellow spheres represent hydrophobic features and the red sphere represents a hydrogen bond acceptor. On the stick model, red represents oxygen atoms, blue represents nitrogen atoms, green represents halogen atoms, and the rest are carbons. Both hydrophobic features align with methyl groups and the hydrogen bond acceptor aligns with a ketone group. Hydrogen atoms are not displayed for clarity.

Figure 6. Receiver operating characteristic (ROC) curve of pharmacophore model of MRP4 inhibitors from virtually screening the test set (N = 77 compounds).

Figure 7. Structural alignment of glucocorticoids clobetasol propionate (orange) and dexamethasone (gray). Clobetasol propionate, a potent MRP4 inhibitor, inhibits MRP4-mediated transport of DHEAS by 101 ± 23%. In contrast, dexamethasone exhibits no significant inhibitory effect (5 ± 34% inhibition). The orange circles indicate identical chemical groups in proximity with each other. On the stick model, red represents oxygen atoms, green represents halogen atoms, and the rest represents carbon atoms.

Figure 8. MRP4: Comparison of calculated LogP of compounds classified as inactive (<21% MRP4 inhibitory activity; n=37) compared to those classified as active (≥21% MRP4 inhibitory activity; n=50). The mean and median LogP values of the inactives are 0.38 and 0.69, respectively, and 3.64 and 3.84, respectively, for the actives.

Figure 9. DHEAS, an MRP4 substrate, and felbinac, an MRP4 inhibitor, aligned with the MRP4 inhibitor pharmacophore. Both compounds also are depicted with their individual

pharmacophore, which shows all possible intermolecular interactions. **A**, DHEAS aligned to the MRP4 pharmacophore. **B**, DHEAS pharmacophore showing all possible intermolecular interactions. **C**, felbinac aligned to the MRP4 pharmacophore. **D**, felbinac pharmacophore showing all possible interactions. Yellow spheres represent hydrophobic features, red spheres represent hydrogen bond acceptor features, the red star represents a negatively ionizable feature, and the purple torus represents an aromatic ring feature. On the stick-models, red represents oxygen atoms, yellow represents phosphorus atoms, and the rest represents carbon atoms. Hydrogen atoms are not displayed for clarity.

DMD Fast Forward. Published on March 3, 2015 as DOI: 10.1124/dmd.114.062539
This article has not been copyedited and formatted. The final version may differ from this version.

Table 1. Composition of Training and Test Set

Transport Model	MRP4	BSEP
Training Set Total (Inhibitors / Non-inhibitors)	57 (34 / 23)	171 (43 / 128)
Test Set Total (Inhibitors / Non-inhibitors)	29 (17 / 12)	86 (22 / 64)
Pharmacophore Training Subset[a]	9	9
Pharmacophore Test Set[b]	77	247

[a] Subset of drugs from the training set used to develop the pharmacophore
[b] Drugs not included in the pharmacophore training set were moved to the test set

DMD Fast Forward. Published on March 3, 2015 as DOI: 10.1124/dmd.114.062539
This article has not been copyedited and formatted. The final version may differ from this version.

Table 2. Characteristics of Bayesian Models for MRP4 and BSEP Inhibition

Bayesian models	MRP4inhib-ECFP_6	MRP4inhib-FCFP_6	BSEPinhib-ECFP_6	BSEPinhib-FCFP_6
2D-fingerprints	ECFP_6	FCFP_6	ECFP_6	FCFP_6
10-Fold XV ROC AUC [a]	0.816	0.793	0.750	0.759
TP/FN/FP/TN [a]	33/1/1/22	33/1/1/22	43/0/3/125	43/0/5/123
External Validation [b]	0.819	0.838	0.845	0.871
TP/FN/FP/TN [b]	8/9/1/11	10/7/2/10	18/4/15/49	17/5/10/54
SE (%)[b]	47.1	58.8	81.8	77.3
SP (%)[b]	91.7	83.3	76.7	84.4
Q (%)[b]	65.5	69.0	77.9	82.6
MCC [b]	0.4123	0.4216	0.5238	0.5796

[a] Cross-validation-based 'receiver operator curve' area under the curve (XV ROC AUC) based on training set compounds (green shaded region).
[b] Predictive performance validation by test set compounds (blue shaded region). True positive (TP), true negative (TN), false positive (FP), false negative (FN), sensitivity (SE), specificity (SP), overall prediction accuracy (Q), and Matthew's correlation coefficient (MCC)(Ung et al., 2007; Khandelwal et al., 2008). SE =TP/(TP + FN), SP = TN/(TN + FP), Q = (TP + TN)/(TP + TN + FP + FN). MCC = $[(TP * TN) - (FN * FP)]/[(TP + FP)(TP + FN)(TN + FN)(TN + FP)]^{1/2}$

Figure 1

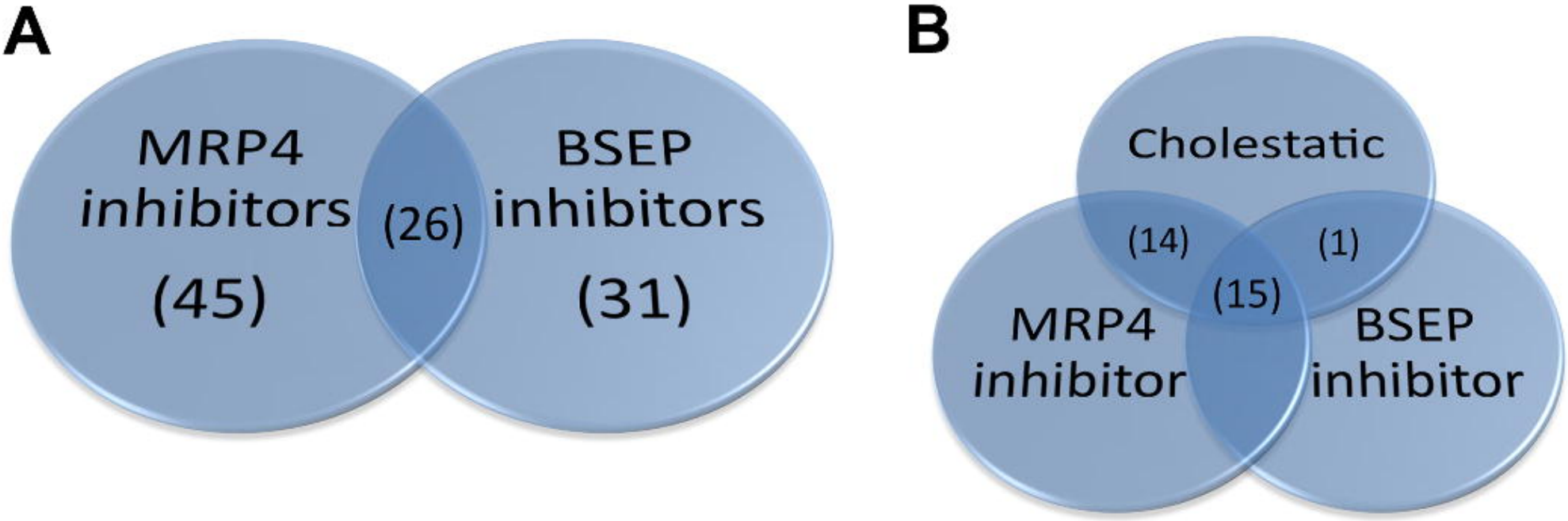
A
MRP4
inhibitors
(45)
(26)
BSEP
inhibitors
(31)
B
Cholestatic
(14)
(1)
(15)
MRP4
inhibitor
BSEP
inhibitor

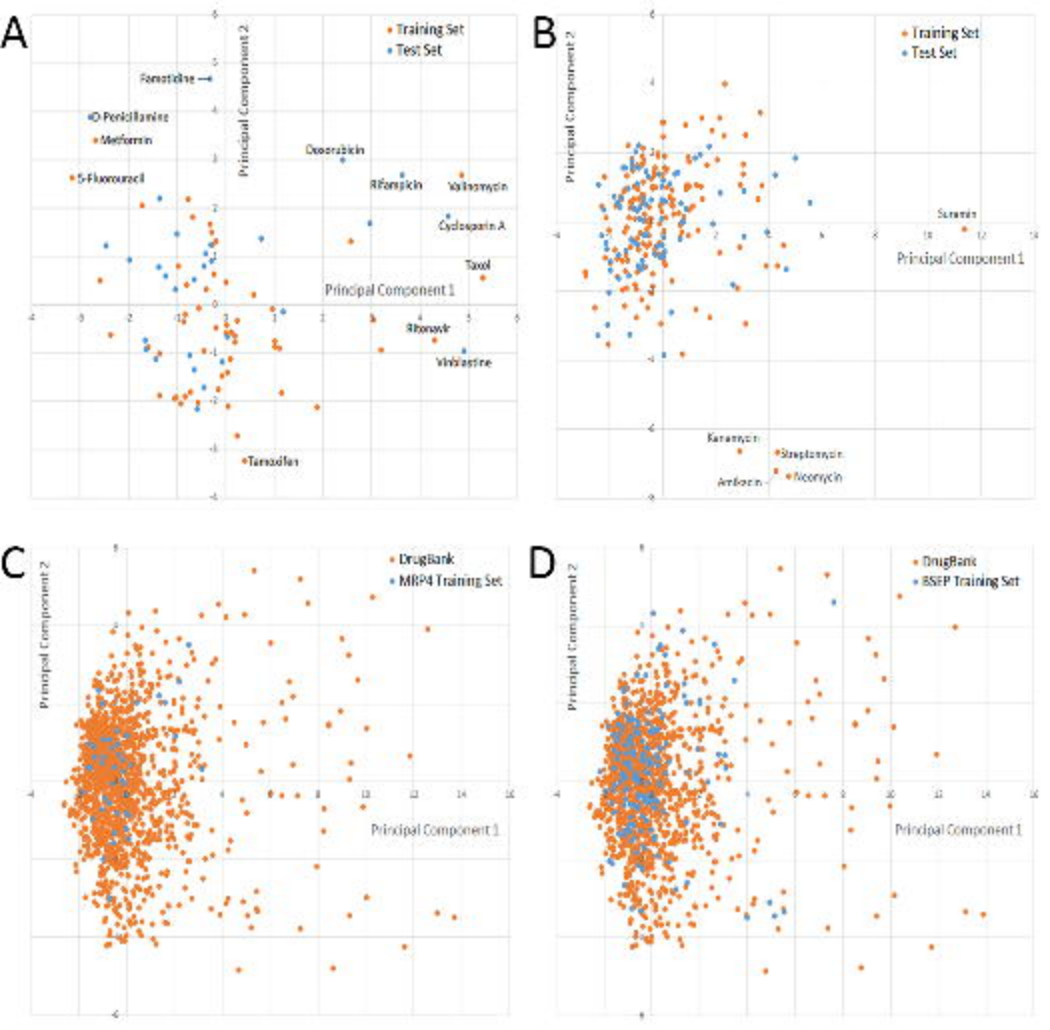
A
Training Set
Test Set
Principal Component 2
Principal Component 1
Famotidine
D-Penicillamine
Metformin
5-Fluorouracil
Doxorubicin
Rifampicin
Valinomycin
Cyclosporin A
Taxol
Rhonwle
Vinblastine
Tamoxifen
B
Training Set
Test Set
Principal Component 2
Principal Component 1
Suramin
Kanamycin
Streptomycin
Amikacin
Neomycin
C
DrugBank
MRP4 Training Set
Principal Component 2
Principal Component 1
D
DrugBank
BSEP Training Set
Principal Component 2
Principal Component 1

Figure 2

Category BayesianModel-MRP4_inhib_FCFP_6: good features from FCFP_6

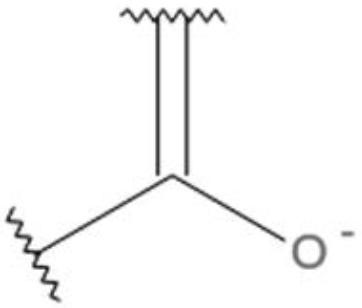

G1: 260714409
6 out of 6 good
Bayesian Score: 0.383

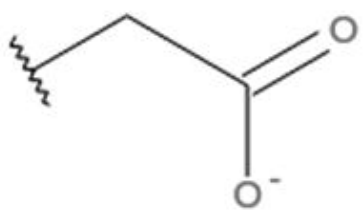

G2: -367494947
6 out of 6 good
Bayesian Score: 0.383

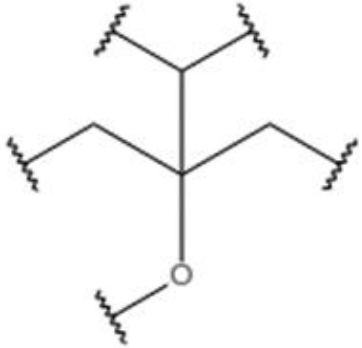

G3: -415216134
5 out of 5 good
Bayesian Score: 0.370

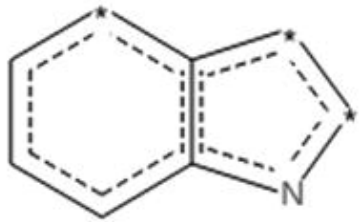

G4: 713358128
5 out of 5 good
Bayesian Score: 0.370

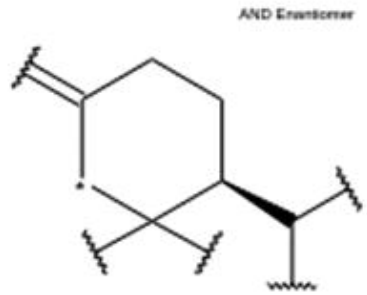

G5: -55265897
5 out of 5 good
Bayesian Score: 0.370

Category BayesianModel-MRP4_inhib_FCFP_6: bad features from FCFP_6

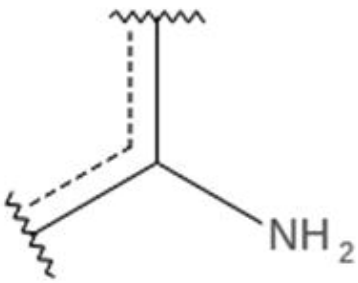

B1: 1069584379
0 out of 4 good
Bayesian Score: -1.257

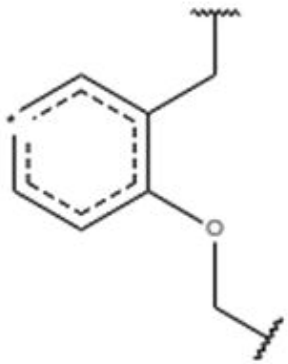

B2: -1099193755
0 out of 4 good
Bayesian Score: -1.257

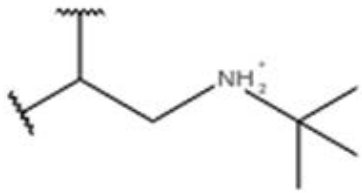

B3: 692823813
0 out of 3 good
Bayesian Score: -1.060

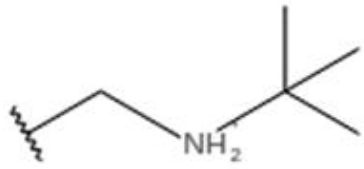

B4: 1995860413
0 out of 3 good
Bayesian Score: -1.060

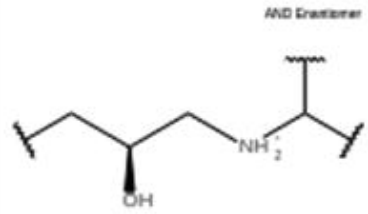

B5: 545355516
0 out of 3 good
Bayesian Score: -1.060

Figure 3

Category BayesianModel-BSEPinhib-FCFP_6: good features from FCFP_6

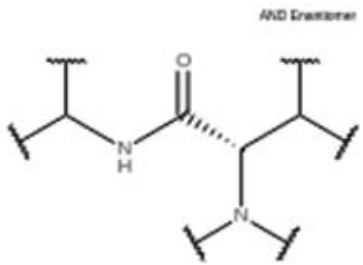

G1: 1862216547
5 out of 5 good
Bayesian Score: 0.816

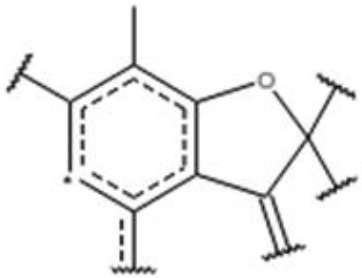

G2: -1096767684
4 out of 4 good
Bayesian Score: 0.767

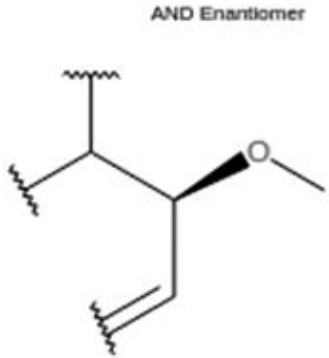

G3: 346066116
4 out of 4 good
Bayesian Score: 0.767

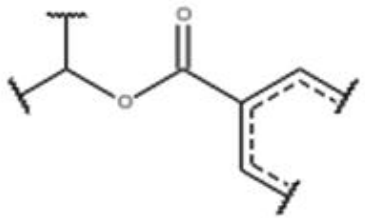

G4: 391786003
4 out of 4 good
Bayesian Score: 0.767

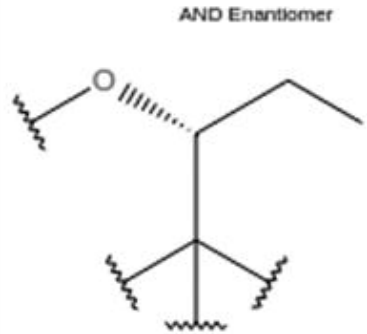

G5: -1576063084
3 out of 3 good
Bayesian Score: 0.697

Category BayesianModel-BSEPinhib-FCFP_6: bad features from FCFP_6

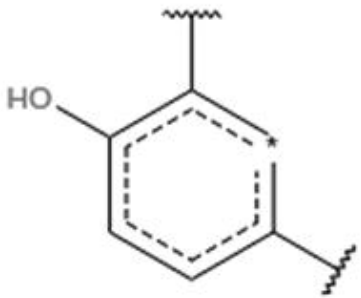

B1: 946589555
0 out of 12 good
Bayesian Score: -1.603

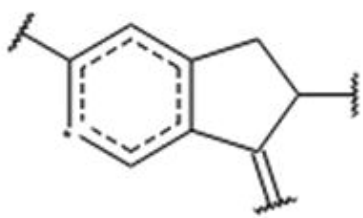

B2: -1943140669
0 out of 10 good
Bayesian Score: -1.460

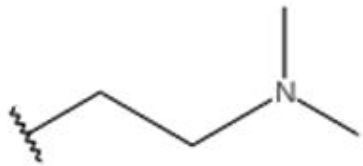

B3: -14048077
0 out of 8 good
Bayesian Score: -1.293

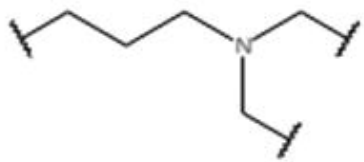

B4: 309602933
2 out of 26 good
Bayesian Score: -1.163

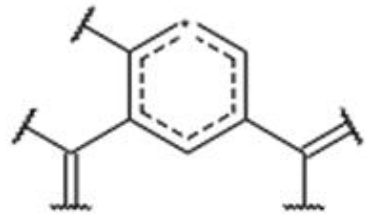

B5: -451251206
0 out of 6 good
Bayesian Score: -1.093

Figure 4

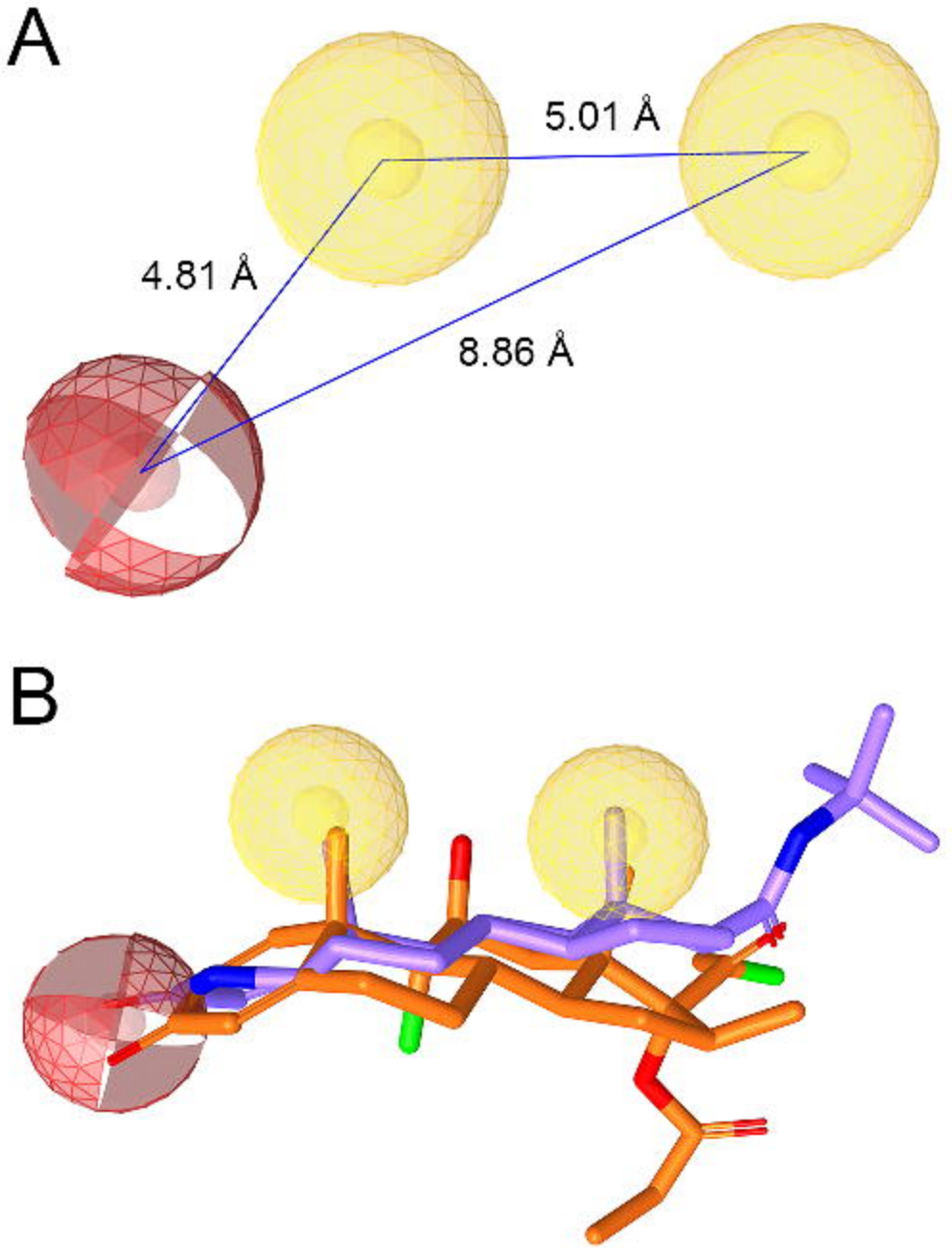

Figure 5

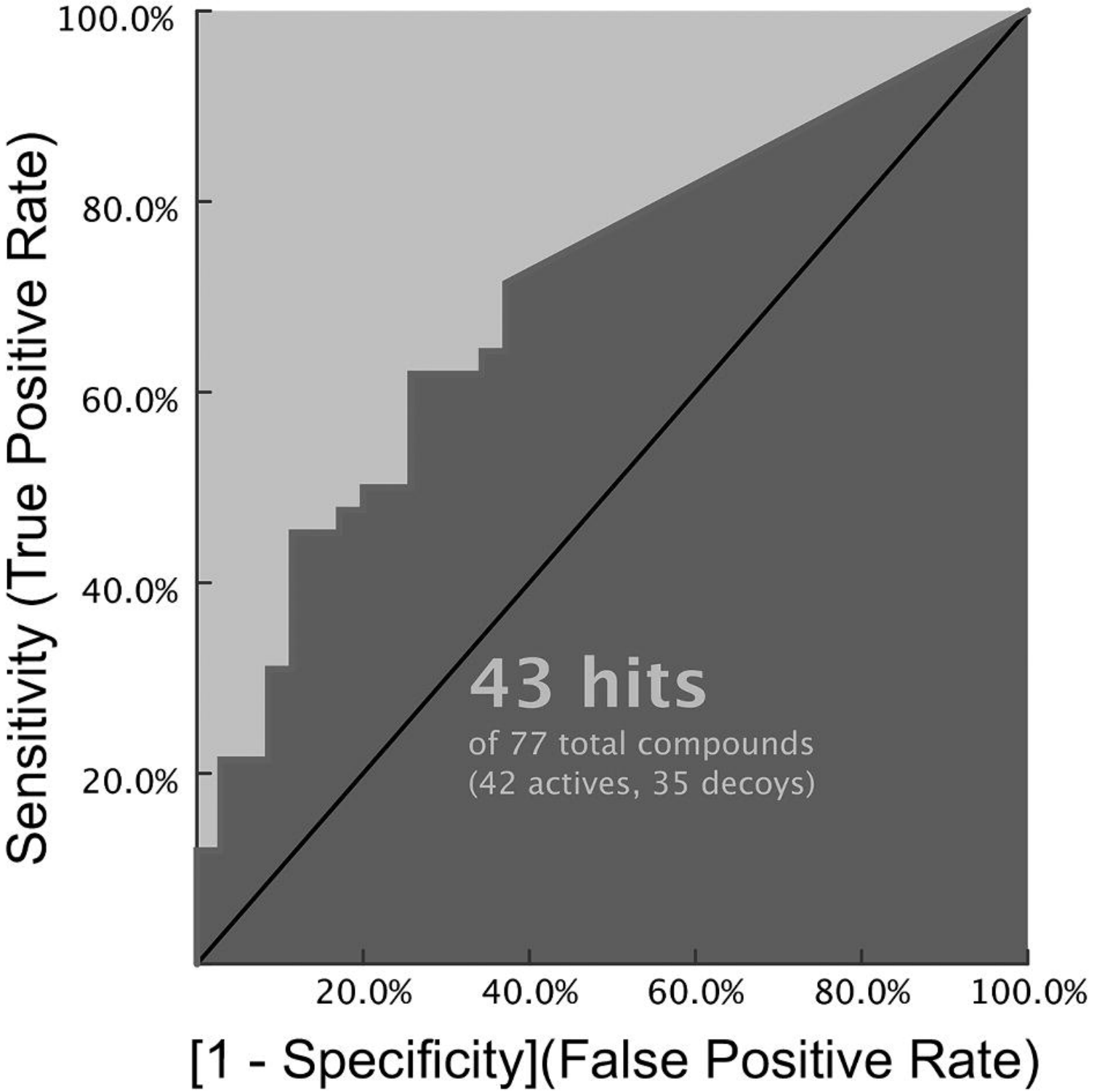
100.0%
80.0%
60.0%
40.0%
20.0%
Sensitivity (True Positive Rate)
43 hits
of 77 total compounds
(42 actives, 35 decoys)
20.0%
40.0%
60.0%
80.0%
100.0%
[1 - Specificity](False Positive Rate)

Figure 6

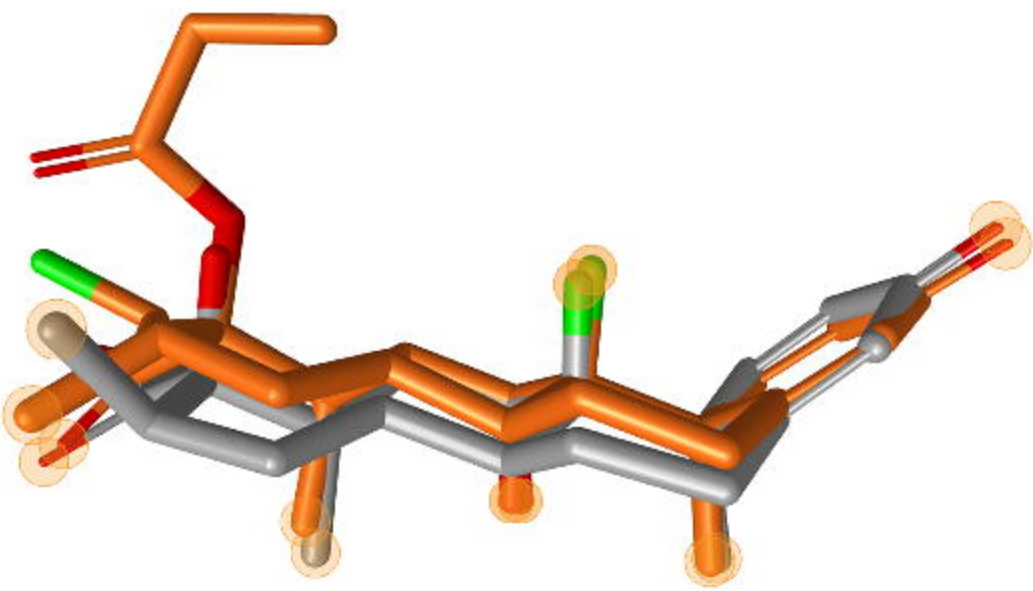

Figure 7

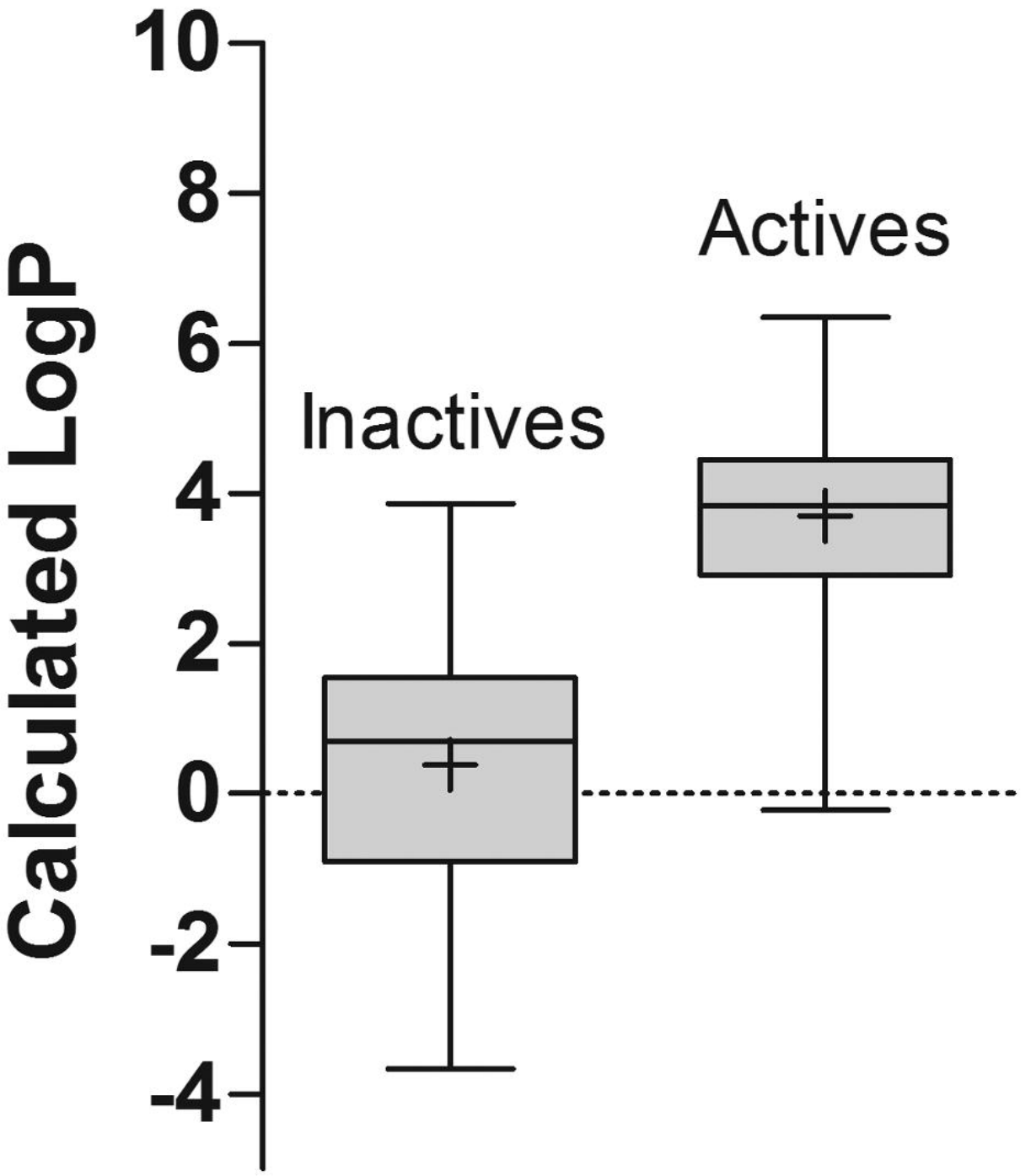

Figure 8

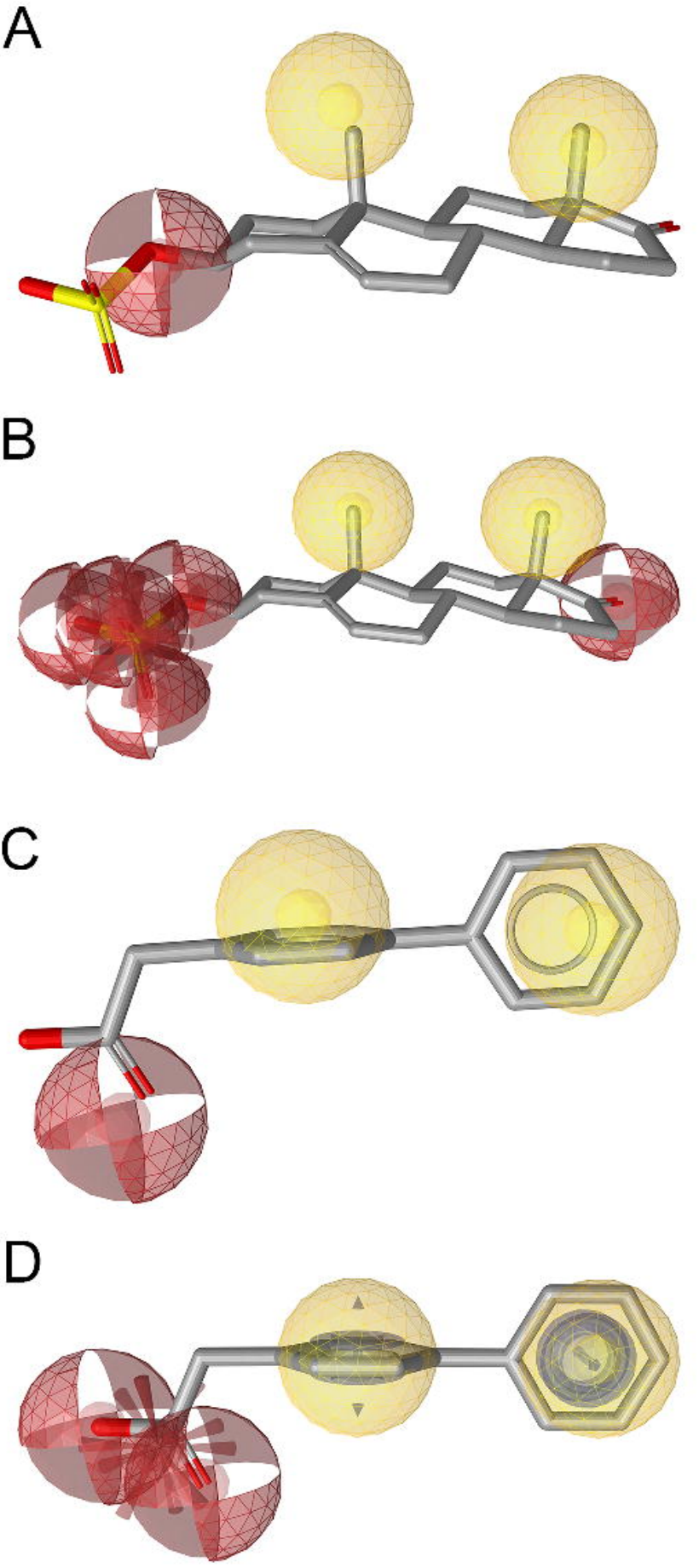

Figure 9

Towards Predicting Drug-Induced Liver Injury (DILI): Parallel Computational Approaches to Identify MRP4 and BSEP Inhibitors

Matthew A. Welch, Kathleen Köck, Thomas J. Urban, Kim L. R. Brouwer, and Peter W. Swaan

Drug Metabolism and Disposition

Supplemental Data

This Supplemental Information includes 1) the drugs which were part of the MRP4 dataset and the BSEP dataset and whether they were included in the training set. 2) The BSEP pharmacophore with the feature distances shown and the BSEP pharmacophore with β-Estradiol 17-(β-D-glucuronide) aligned. 3) The expanded figure showing the favorable and unfavorable fingerprints for MRP4 and BSEP for both the ECFP_6 and FCFP_6 model.

Supplementary Table S1.

These two tables contain the names of the drugs in the MRP4 dataset and BSEP dataset, PubChem ID or CHEMBL ID if available, the inhibition data, and the compound's classification for the model. Drugs with a "TRUE" value for the training set column were used to train the Bayesian model and those with a "FALSE" value were part of the test set used to validate the model. The IC50 values for the BSEP dataset were derived from Morgan et al., Toxicol Sci. 2013 and Dawson et al., Drug Metab Dispos. 2012. The active classification category indicates if the molecules were considered active or inactive which is ≥21% for MRP4 inhibition or an IC_{50} <133 for BSEP.

MRP4 Dataset

Name	PUBCHEM CID	MRP4 TrainingSet	MRP4 % Inhibition	Active Classification
Sulindac	1548887	TRUE	112	TRUE
Trimethoprim	5578	TRUE	9	FALSE
Chloramphenicol	5959	TRUE	6	FALSE
Metoclopramide	4168	TRUE	-12	FALSE
Clopamide	2804	TRUE	10	FALSE
Furosemide	3440	TRUE	109	TRUE
Haloperidol	3559	TRUE	34	TRUE
Chlorpromazine	2726	TRUE	84	TRUE
Etoposide	36462	TRUE	33	TRUE
Verapamil	2520	TRUE	44	TRUE
Lopinavir	92727	TRUE	76	TRUE
Ritonavir	392622	TRUE	72	TRUE
Sorafenib	216239	TRUE	121	TRUE
Tacrine	1935	TRUE	6	FALSE
Buspirone	2477	TRUE	13	FALSE
Timolol	33624	TRUE	12	FALSE
Quinine	8549	TRUE	41	TRUE
Oxybutynin	4634	TRUE	67	TRUE
Alprenolol	2119	TRUE	10	FALSE
Nadolol	39147	TRUE	-25	FALSE
Indomethacin	3715	TRUE	111	TRUE
Vinblastine	13342	TRUE	10	FALSE
Cimetidine	2756	TRUE	0	FALSE
Alpidem	54897	TRUE	47	TRUE
Nortriptyline	4543	TRUE	36	TRUE
Metformin	4091	TRUE	-6	FALSE
Fluvastatin	446155	TRUE	62	TRUE
Tamoxifen	2733526	TRUE	102	TRUE

BSEP Dataset

Name	CHEMBL ID	BSEP TrainingSet	IC_{50}	Active Classification
Acecainide		TRUE	133	FALSE
Antimycin		TRUE	59.6	TRUE
Camptothecin		TRUE	133	FALSE
Fenclozic acid		TRUE	133	FALSE
Quercetin		TRUE	133	FALSE
R-Apomorphine		TRUE	133	FALSE
Selegiline		TRUE	133	FALSE
Sitagliptin		TRUE	133	FALSE
Suramin		TRUE	133	FALSE
Vioxx		TRUE	133	FALSE
Acetaminophen	CHEMBL112	TRUE	1000	FALSE
Acyclovir	CHEMBL184	TRUE	133	FALSE
Alfentanil	CHEMBL634	TRUE	133	FALSE
Amikacin	CHEMBL177	TRUE	133	FALSE
Amitriptyline	CHEMBL629	TRUE	133	FALSE
Amrinone	CHEMBL12856	TRUE	133	FALSE
Atropine	CHEMBL195	TRUE	133	FALSE
Benoxaprofen	CHEMBL340978	TRUE	175	FALSE
Betaine	CHEMBL95889	TRUE	1000	FALSE
Betamipron	CHEMBL1231530	TRUE	133	FALSE
Busulfan	CHEMBL820	TRUE	1000	FALSE
Butorphanol	CHEMBL33986	TRUE	133	FALSE
Cefotetan	CHEMBL474579	TRUE	133	FALSE
Chloroquine	CHEMBL76	TRUE	133	FALSE
Cinchophen	CHEMBL348000	TRUE	695.3	FALSE
Ciprofloxacin	CHEMBL8	TRUE	133	FALSE
Clavulanate	CHEMBL777	TRUE	1000	FALSE
Cloxacillin	CHEMBL891	TRUE	219.7	FALSE

Clobetasol propionate	32798	TRUE	101	TRUE
Terbutaline	5403	TRUE	20	FALSE
Antipyrine	2206	TRUE	-5	FALSE
Naloxone	5284596	TRUE	-7	FALSE
Nitrofurantoin	6604200	TRUE	101	TRUE
Bezafibrate	39042	TRUE	41	TRUE
Indinavir	5362440	TRUE	15	FALSE
Mibefradil	60663	TRUE	91	TRUE
Chlorpheniramine	2725	TRUE	20	FALSE
Fluorescein	16850	TRUE	5	FALSE
Benzbromarone	2333	TRUE	111	TRUE
Finasteride	57363	TRUE	49	TRUE
Tolbutamide	5505	TRUE	-5	FALSE
Dicloxacillin	18381	TRUE	41	TRUE
Primaquine	4908	TRUE	11	FALSE
Diphenhydramine	3100	TRUE	31	TRUE
19-Norethindrone	6230	TRUE	33	TRUE
Fenofibrate	3339	TRUE	39	TRUE
Valinomycin	5649	TRUE	65	TRUE
Glafenine	3474	TRUE	105	TRUE
Flupirtine	53276	TRUE	11	FALSE
Caffeine	2519	TRUE	5	FALSE
Nitrendipine	4507	TRUE	93	TRUE
Pioglitazone	4829	TRUE	34	TRUE
Rosiglitazone	77999	TRUE	88	TRUE
Desipramine	2995	TRUE	27	TRUE
5-Fluorouracil	3385	TRUE	1	FALSE
Simvastatin	54454	TRUE	111	TRUE
Promethazine	4927	TRUE	64	TRUE
Aspirin	2244	FALSE	9	FALSE
Theophylline	2153	FALSE	4	FALSE
Quinidine	441074	FALSE	77	TRUE
Rifamycin SV	6324616	FALSE	75	TRUE
Famotidine	5702160	FALSE	16	FALSE
Glyburide	3488	FALSE	93	TRUE
Tolcapone	4659569	FALSE	113	TRUE
Troglitazone	5591	FALSE	105	TRUE
Acitretin	5284513	FALSE	33	TRUE
Dexmethasone	5743	FALSE	5	FALSE
D-Penicillamine	5852	FALSE	-10	FALSE
Omeprazole	4594	FALSE	21	TRUE
Chlorpropamide	2727	FALSE	-12	FALSE
Doxorubicin	31703	FALSE	12	FALSE
Rifampicin	5381226	FALSE	60	TRUE

Cromolyn	CHEMBL428880	TRUE	1000	FALSE
Cyclophosphamide	CHEMBL88	TRUE	133	FALSE
Dapsone	CHEMBL1043	TRUE	133	FALSE
Diazepam	CHEMBL12	TRUE	133	FALSE
Dihydralazine	CHEMBL35505	TRUE	1000	FALSE
Diltiazem	CHEMBL23	TRUE	133	FALSE
Disopyramide	CHEMBL517	TRUE	133	FALSE
Donepezil	CHEMBL502	TRUE	78	TRUE
Doxepin	CHEMBL101740	TRUE	133	FALSE
Eprosartan	CHEMBL813	TRUE	133	FALSE
Ethinylestradiol	CHEMBL1078384	TRUE	14	TRUE
Etoricoxib	CHEMBL416146	TRUE	53.2	TRUE
Flumazenil	CHEMBL407	TRUE	133	FALSE
Flutamide	CHEMBL806	TRUE	133	FALSE
Ganciclovir	CHEMBL182	TRUE	133	FALSE
Gemfibrozil	CHEMBL457	TRUE	133	FALSE
Glipizide	CHEMBL1073	TRUE	133	FALSE
Guanfacine	CHEMBL862	TRUE	133	FALSE
Idazoxan	CHEMBL10316	TRUE	133	FALSE
Indoramin	CHEMBL279516	TRUE	133	FALSE
Iproniazide	CHEMBL92401	TRUE	1000	FALSE
Isoproterenol	CHEMBL434	TRUE	1000	FALSE
Kanamycin	CHEMBL176	TRUE	133	FALSE
Ketanserin	CHEMBL51	TRUE	133	FALSE
Ketotifen	CHEMBL534	TRUE	738.4	FALSE
Leflunomide	CHEMBL960	TRUE	133	FALSE
Levofloxacin	CHEMBL33	TRUE	133	FALSE
Methapyrilene	CHEMBL1411979	TRUE	1000	FALSE
Methimazole	CHEMBL1515	TRUE	133	FALSE
Methylprednisolone	CHEMBL650	TRUE	133	FALSE
Metocurine	CHEMBL1259	TRUE	133	FALSE
Metoprolol	CHEMBL13	TRUE	133	FALSE
MK-571	CHEMBL15177	TRUE	3.53	TRUE
Moclobemide	CHEMBL86304	TRUE	133	FALSE
Morphine	CHEMBL70	TRUE	133	FALSE
Naproxen	CHEMBL154	TRUE	133	FALSE
Neomycin	CHEMBL449118	TRUE	133	FALSE
Neostigmine	CHEMBL278020	TRUE	133	FALSE
Nicotine	CHEMBL3	TRUE	133	FALSE
Nimodipine	CHEMBL1428	TRUE	133	FALSE
Nomifensine	CHEMBL273575	TRUE	1000	FALSE
Ondansetron	CHEMBL46	TRUE	133	FALSE
Papaverine	CHEMBL19224	TRUE	133	FALSE
Pefloxacin	CHEMBL267648	TRUE	133	FALSE

Sulfasalazine	5353980	FALSE	118	TRUE
Fluoxetine	3386	FALSE	70	TRUE
Ranitidine	3001055	FALSE	10	FALSE
Cyclosporin A	5284373	FALSE	23	TRUE
Ticlopidine	5472	FALSE	35	TRUE
Phenformin	8249	FALSE	20	FALSE
Clozapine	2818	FALSE	25	TRUE
Maprotiline	4011	FALSE	29	TRUE
Carbamazepine	2554	FALSE	-3	FALSE
Probenecid	4911	FALSE	8	FALSE
Nifedipine	4485	FALSE	46	TRUE
Praziquantel	4891	FALSE	59	TRUE
Ibuprofen	3672	FALSE	39	TRUE
Triamterene	5546	FALSE	31	FALSE

Pentamidine	CHEMBL55	TRUE	133	FALSE
Phenacetin	CHEMBL16073	TRUE	133	FALSE
Physostigmine	CHEMBL94	TRUE	1000	FALSE
Picotamide	CHEMBL1257015	TRUE	441	FALSE
Pindolol	CHEMBL500	TRUE	133	FALSE
Practolol	CHEMBL6995	TRUE	1000	FALSE
Prednisolone	CHEMBL131	TRUE	133	FALSE
Prochlorperazine	CHEMBL728	TRUE	133	FALSE
Pyridoxine	CHEMBL1364	TRUE	1000	FALSE
Remoxipride	CHEMBL22242	TRUE	133	FALSE
Risperidone	CHEMBL85	TRUE	133	FALSE
Streptomycin	CHEMBL1201194	TRUE	1000	FALSE
Sulfadiazine	CHEMBL439	TRUE	133	FALSE
Sumatriptan	CHEMBL128	TRUE	133	FALSE
Tenoxicam	CHEMBL487234	TRUE	133	FALSE
Tetracycline	CHEMBL1440	TRUE	133	FALSE
Tizanidine	CHEMBL1079	TRUE	133	FALSE
Trazodone	CHEMBL621	TRUE	133	FALSE
Tubocurarine	CHEMBL339427	TRUE	133	FALSE
Urapidil	CHEMBL279229	TRUE	133	FALSE
Venlafaxine	CHEMBL637	TRUE	133	FALSE
Zileuton	CHEMBL93	TRUE	133	FALSE
Zonisamide	CHEMBL750	TRUE	133	FALSE
5-Fluorouracil	CHEMBL185	TRUE	133	FALSE
Aspirin	CHEMBL25	TRUE	133	FALSE
Carbamazepine	CHEMBL108	TRUE	133	FALSE
Chloramphenicol	CHEMBL130	TRUE	133	FALSE
Chlorpropamide	CHEMBL498	TRUE	133	FALSE
Cimetidine	CHEMBL30	TRUE	133	FALSE
Clopamide	CHEMBL1361347	TRUE	133	FALSE
D-penicillamine	CHEMBL1430	TRUE	1000	FALSE
Dexamethasone	CHEMBL384467	TRUE	133	FALSE
Doxorubicin	CHEMBL179	TRUE	133	FALSE
Famotidine	CHEMBL902	TRUE	133	FALSE
Fluorescein	CHEMBL177756	TRUE	133	FALSE
Maprotiline	CHEMBL21731	TRUE	133	FALSE
Naloxone	CHEMBL80	TRUE	133	FALSE
Phenformin	CHEMBL170988	TRUE	133	FALSE
Probenecid	CHEMBL897	TRUE	133	FALSE
Theophylline	CHEMBL190	TRUE	133	FALSE
Timolol	CHEMBL499	TRUE	133	FALSE
Bezafibrate	CHEMBL264374	TRUE	231.7	FALSE
Chlorpromazine	CHEMBL71	TRUE	133	FALSE
Furosemide	CHEMBL35	TRUE	133	FALSE

Ibuprofen	CHEMBL175	TRUE	598.6	FALSE
Nitrofurantoin	CHEMBL572	TRUE	133	FALSE
Promethazine	CHEMBL643	TRUE	133	FALSE
Quinine	CHEMBL170	TRUE	133	FALSE
Sulfasalazine	CHEMBL421	TRUE	133	FALSE
Sulindac	CHEMBL15770	TRUE	133	FALSE
Tamoxifen	CHEMBL83	TRUE	133	FALSE
Triamterene	CHEMBL585	TRUE	133	FALSE
Vinblastine	CHEMBL159	TRUE	133	FALSE
Cycloserine	CHEMBL771	TRUE	1000	FALSE
Zoledronic acid	CHEMBL924	TRUE	133	FALSE
Verapamil	CHEMBL197	TRUE	133	FALSE
Staurosporine		TRUE	18.7	TRUE
Amiodarone	CHEMBL633	TRUE	43	TRUE
Bosentan	CHEMBL957	TRUE	23	TRUE
Chlordiazepoxide	CHEMBL451	TRUE	44.1	TRUE
Cinnarizine	CHEMBL43064	TRUE	15.7	TRUE
Clofazimine	CHEMBL1292	TRUE	12.9	TRUE
Clofibrate	CHEMBL565	TRUE	71	TRUE
Gefitinib	CHEMBL939	TRUE	10.9	TRUE
Imatinib	CHEMBL941	TRUE	25.1	TRUE
Itraconazole	CHEMBL22587	TRUE	18	TRUE
Midazolam	CHEMBL655	TRUE	41.74	TRUE
Nefazodone	CHEMBL623	TRUE	6.11	TRUE
Nicardipine	CHEMBL1484	TRUE	7.87	TRUE
Norethindrone	CHEMBL1162	TRUE	55	TRUE
Pazopanib	CHEMBL477772	TRUE	10.3	TRUE
Reserpine	CHEMBL772	TRUE	8.35	TRUE
Saquinavir	CHEMBL114	TRUE	4.9	TRUE
Telithromycin	CHEMBL1136	TRUE	5	TRUE
Telmisartan	CHEMBL1017	TRUE	16.2	TRUE
Wortmannin	CHEMBL428496	TRUE	13.6	TRUE
Cyclosporine A	CHEMBL160	TRUE	0.5	TRUE
Flupirtine	CHEMBL255044	TRUE	35.5	TRUE
Omeprazole	CHEMBL1344	TRUE	99	TRUE
Primaquine	CHEMBL506	TRUE	32.7	TRUE
Alpidem	CHEMBL54349	TRUE	9.2	TRUE
Benzbromarone	CHEMBL388590	TRUE	17.5	TRUE
Dicloxacillin	CHEMBL893	TRUE	56.4	TRUE
Erythromycin estolate	CHEMBL1200688	TRUE	13	TRUE
Fenofibrate	CHEMBL672	TRUE	15.3	TRUE
Fluvastatin	CHEMBL1078	TRUE	36.1	TRUE
Glafenine	CHEMBL146095	TRUE	22.3	TRUE
Glyburide	CHEMBL472	TRUE	5	TRUE

Indomethacin	CHEMBL6	TRUE	42	TRUE
Lopinavir	CHEMBL729	TRUE	17.3	TRUE
Nifedipine	CHEMBL193	TRUE	63.9	TRUE
Pioglitazone	CHEMBL595	TRUE	0.4	TRUE
Rifampin SV	CHEMBL180	TRUE	11.3	TRUE
Rifamycin Sv	CHEMBL437765	TRUE	6.3	TRUE
Rosiglitazone	CHEMBL121	TRUE	2.8	TRUE
Sorafenib	CHEMBL1336	TRUE	8	TRUE
Tolcapone	CHEMBL1324	TRUE	36.6	TRUE
Troglitazone	CHEMBL408	TRUE	3	TRUE
Taxol	CHEMBL48	TRUE	15	TRUE
Glimepiride		FALSE	15.7	TRUE
Amprenavir	CHEMBL116	FALSE	44.8	TRUE
Drotaverine	CHEMBL551978	FALSE	37	TRUE
Fusidic Acid	CHEMBL374975	FALSE	10.1	TRUE
Ketoconazole	CHEMBL75	FALSE	3.4	TRUE
Nelfinavir	CHEMBL1159655	FALSE	11.8	TRUE
Rifabutin	CHEMBL444633	FALSE	26.7	TRUE
Buspirone	CHEMBL49	FALSE	104.5	TRUE
Clozapine	CHEMBL42	FALSE	133	FALSE
Indinavir	CHEMBL115	FALSE	21.2	TRUE
Acitretin	CHEMBL1131	FALSE	38.2	TRUE
Clobetasol Propionate	CHEMBL1159650	FALSE	8.5	TRUE
Finasteride	CHEMBL710	FALSE	28.2	TRUE
Mibefradil	CHEMBL45816	FALSE	<135	FALSE
Nitrendipine	CHEMBL475534	FALSE	22.5	TRUE
Oxybutynin	CHEMBL1231	FALSE	27.4	TRUE
Praziquantel	CHEMBL976	FALSE	67.1	TRUE
Ritonavir	CHEMBL163	FALSE	1.74	TRUE
Simvastatin	CHEMBL1064	FALSE	24.7	TRUE
Ticlopidine	CHEMBL833	FALSE	74	TRUE
Valinomycin	CHEMBL223643	FALSE	1.56	TRUE
Lapatinib	CHEMBL554	FALSE	6.49	TRUE
ANIT		FALSE	69	TRUE
Ciglitazone		FALSE	37.8	TRUE
Acetazolamide	CHEMBL20	FALSE	133	FALSE
Amoxicillin	CHEMBL1082	FALSE	133	FALSE
Azathioprine	CHEMBL1542	FALSE	133	FALSE
Betamethasone	CHEMBL632	FALSE	133	FALSE
Bumetanide	CHEMBL1072	FALSE	133	FALSE
Carmustine	CHEMBL513	FALSE	133	FALSE
Chlorambucil	CHEMBL515	FALSE	133	FALSE
Ciprofibrate	CHEMBL557555	FALSE	133	FALSE
Clomipramine	CHEMBL415	FALSE	133	FALSE

Colchicine	CHEMBL107	FALSE	133	FALSE
Diazoxide	CHEMBL181	FALSE	133	FALSE
Dopamine	CHEMBL59	FALSE	1000	FALSE
Emetine	CHEMBL50588	FALSE	133	FALSE
Felbamate	CHEMBL1094	FALSE	1000	FALSE
Flucloxacillin	CHEMBL222645	FALSE	208.6	FALSE
Galantamine	CHEMBL659	FALSE	133	FALSE
Gliclazide	CHEMBL427216	FALSE	133	FALSE
Imipramine	CHEMBL11	FALSE	133	FALSE
Isoniazid	CHEMBL64	FALSE	133	FALSE
Ketamine	CHEMBL742	FALSE	133	FALSE
Lansoprazole	CHEMBL480	FALSE	133	FALSE
Lidocaine	CHEMBL79	FALSE	133	FALSE
Methotrexate	CHEMBL426	FALSE	133	FALSE
Minoxidil	CHEMBL802	FALSE	133	FALSE
Nefopam	CHEMBL465026	FALSE	133	FALSE
Nevirapine	CHEMBL57	FALSE	133	FALSE
Nitrazepam	CHEMBL13209	FALSE	133	FALSE
Pargyline	CHEMBL673	FALSE	1000	FALSE
Perphenazine	CHEMBL567	FALSE	133	FALSE
Phenobarbital	CHEMBL40	FALSE	133	FALSE
Pinacidil	CHEMBL1159	FALSE	348.1	FALSE
Prazosin	CHEMBL2	FALSE	133	FALSE
Procainamide	CHEMBL640	FALSE	133	FALSE
Propranolol	CHEMBL27	FALSE	133	FALSE
Salicylic acid	CHEMBL424	FALSE	1000	FALSE
Sotalol	CHEMBL471	FALSE	133	FALSE
Sulfamethoxazole	CHEMBL443	FALSE	133	FALSE
Sulpiride	CHEMBL26	FALSE	1000	FALSE
Thiotepa	CHEMBL671	FALSE	133	FALSE
Valproate	CHEMBL109	FALSE	1000	FALSE
Alprenolol	CHEMBL266195	FALSE	133	FALSE
Antipyrine	CHEMBL277474	FALSE	133	FALSE
Caffeine	CHEMBL113	FALSE	133	FALSE
Chlorpheniramine	CHEMBL505	FALSE	133	FALSE
Desipramine	CHEMBL72	FALSE	133	FALSE
Metformin	CHEMBL1431	FALSE	133	FALSE
Metoclopramide	CHEMBL86	FALSE	133	FALSE
Nadolol	CHEMBL649	FALSE	133	FALSE
Ranitidine	CHEMBL1790041	FALSE	133	FALSE
Tacrine	CHEMBL95	FALSE	133	FALSE
Terbutaline	CHEMBL1760	FALSE	133	FALSE
Tolbutamide	CHEMBL782	FALSE	133	FALSE
Trimethoprim	CHEMBL22	FALSE	133	FALSE

Diphenhydramine	CHEMBL657	FALSE	133	FALSE
Etoposide	CHEMBL44657	FALSE	133	FALSE
Fluoxetine	CHEMBL41	FALSE	133	FALSE
Haloperidol	CHEMBL54	FALSE	133	FALSE
Nortriptyline	CHEMBL445	FALSE	133	FALSE
Quinidine	CHEMBL97	FALSE	133	FALSE
Fialuridine		FALSE	1000	FALSE
Cefixime	CHEMBL1541	FALSE	133	FALSE
Methyldopa	CHEMBL459	FALSE	1000	FALSE

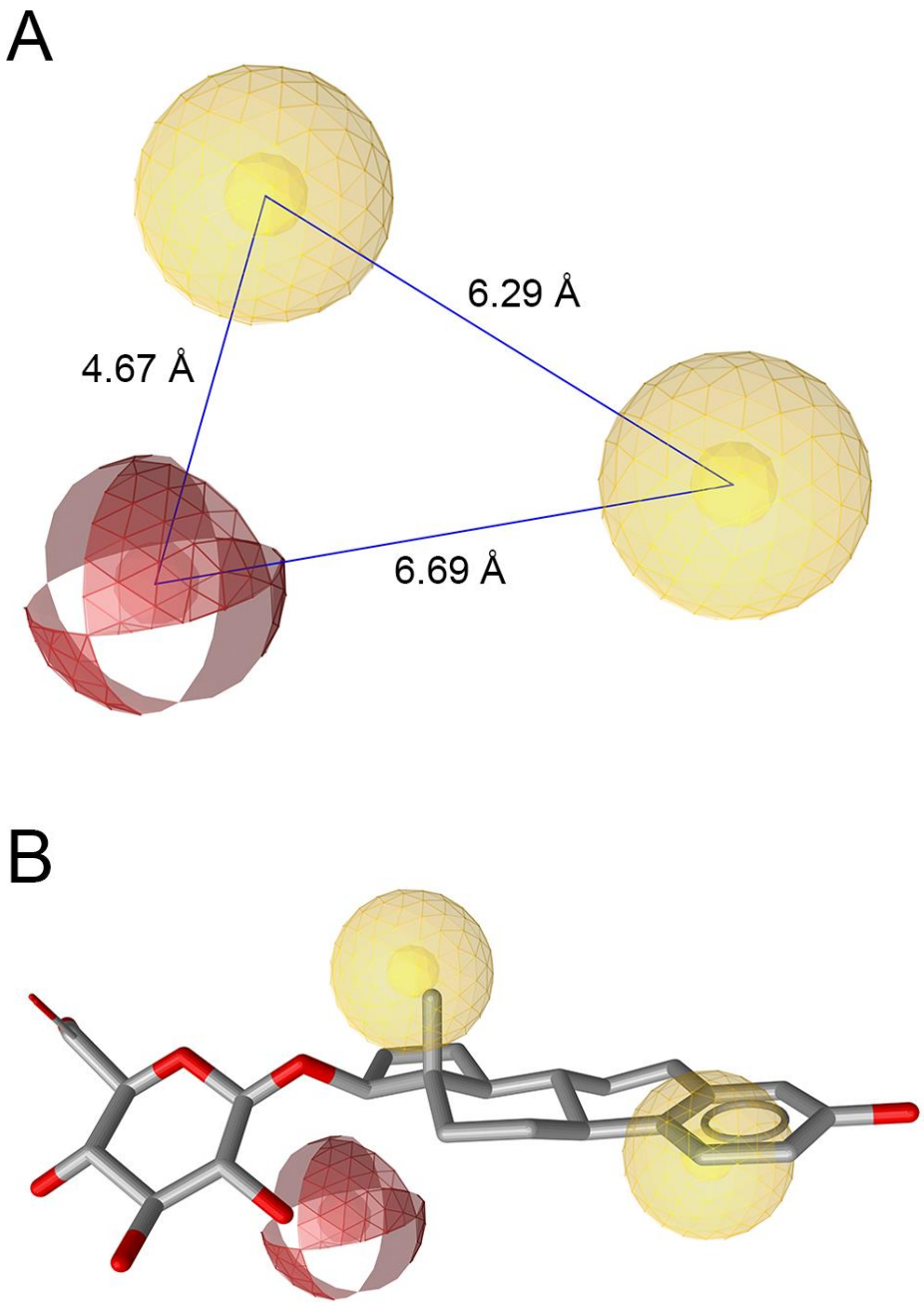

Supplementary Figure S1.

The BSEP pharmacophore and the assay substrate aligned to the BSEP pharmacophore. **A**, the BSEP pharmacophore with the feature distances shown. The yellow spheres represent hydrophobic features and the red sphere represents a hydrogen bond acceptor feature. **B**, the BSEP pharmacophore with β-Estradiol 17-(β-D-glucuronide), the MRP4 substrate used to produce the BSEP inhibitor data, aligned to the pharmacophore.

Category BayesianModel-MRP4_inhib_ECFP_6: good features from ECFP_6

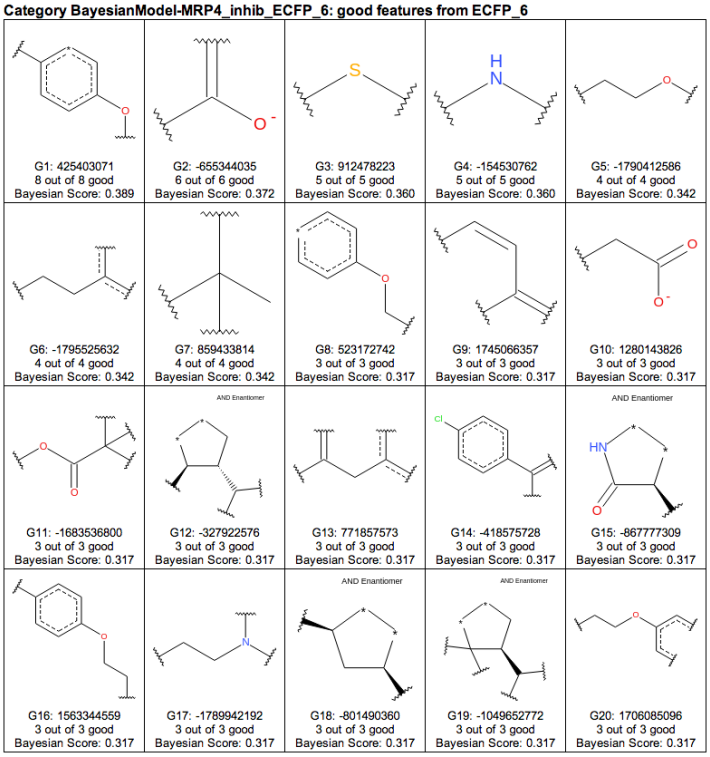

Category BayesianModel-MRP4_inhib_ECFP_6: bad features from ECFP_6

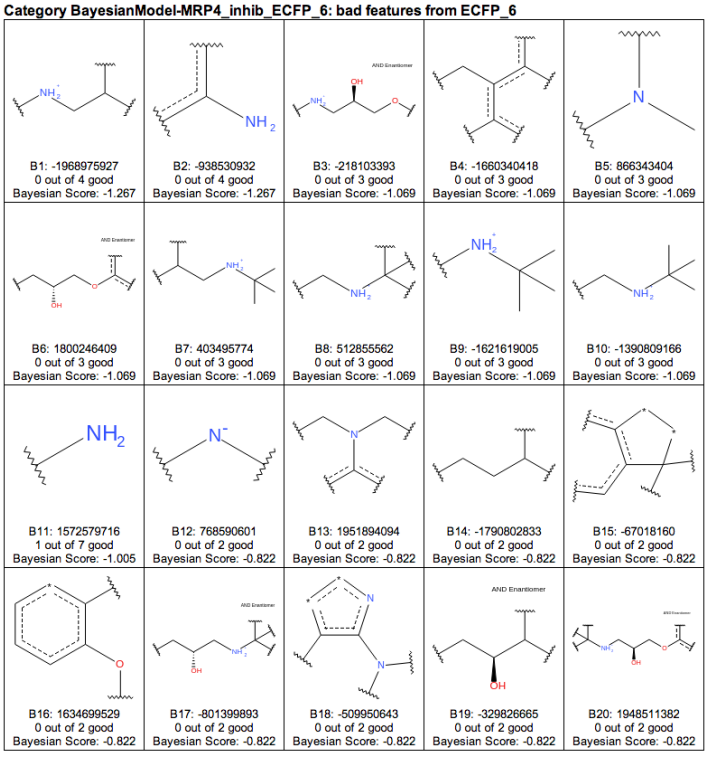

Category BayesianModel-MRP4_inhib_FCFP_6: good features from FCFP_6

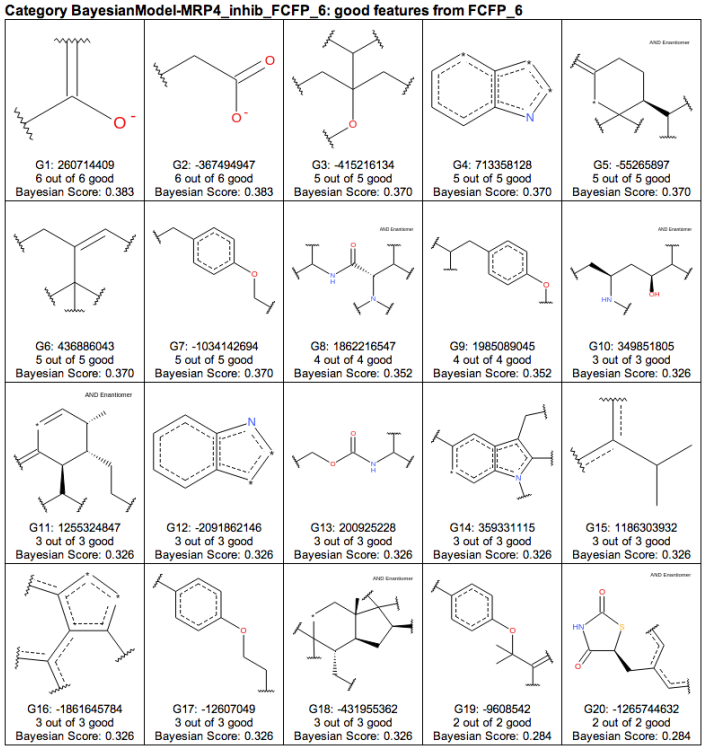

Category BayesianModel-MRP4_inhib_FCFP_6: bad features from FCFP_6

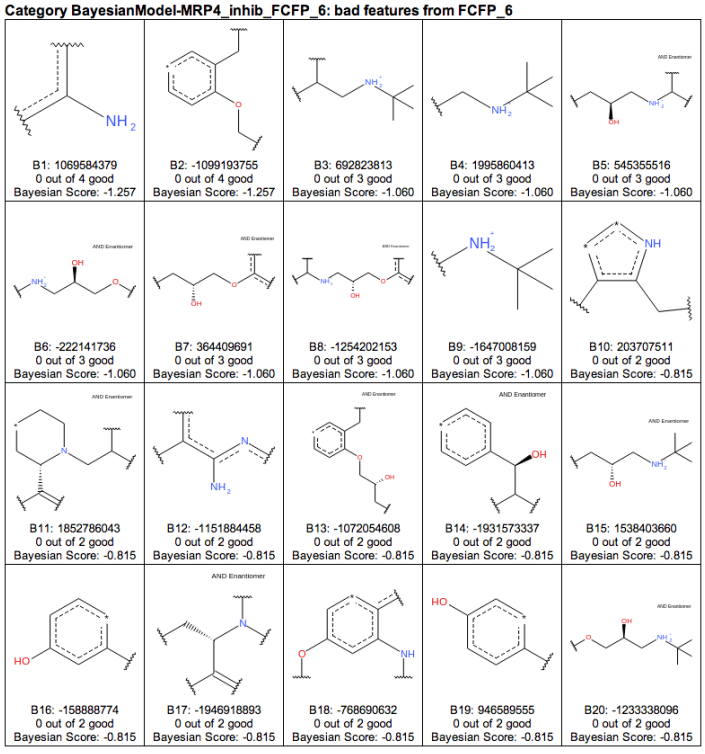

Supplementary Figure S2.

Favorable and unfavorable molecular features for interactions with MRP4 and BSEP. These figures contain the 20 most predictive molecular features for both favorable and unfavorable inhibitory activity against MRP4 and BSEP generated using ECFP_6 and FCFP_6 fingerprints.